INTERNATIONAL CONFERENCE
ELMECO'94

Lublin 8th - 9th September, 1994

ELECTROMAGNETIC DEVICES AND PROCESSES IN ENVIRONMENT PROTECTION

Post-Conference Materials

LUBLIN TECHNICAL UNIVERSITY
DEPARTMENT OF FUNDAMENTAL ELECTRICAL ENGINEERING

Sponsors:

✳ EUROPEAN RESEARCH OFFICE of the UNITED STATES ARMY

✳ TRANS-EUROPEAN MOBILITY SCHEME for UNIVERSITY STUDIES
TEMPUS JEN N°00112-93

INTERNATIONAL CONFERENCE
ELMECO'94

Lublin 8th - 9th September, 1994

ELECTROMAGNETIC DEVICES AND PROCESSES IN ENVIRONMENT PROTECTION

Post-Conference Materials

LUBLIN TECHNICAL UNIVERSITY
DEPARTMENT OF FUNDAMENTAL ELECTRICAL ENGINEERING

Sponsors:

✳ EUROPEAN RESEARCH OFFICE of the UNITED STATES ARMY

✳ TRANS-EUROPEAN MOBILITY SCHEME for UNIVERSITY STUDIES
TEMPUS JEN N°00112-93

ELMECO'94

Hosted by:
Dept. of Fundamental Electrical Engineering
Lublin Technical University
ul. Nadbystrzycka 38a,20 - 618 Lublin
Poland
tel/fax: 0048 - 81 - 553694
e-mail: ELMECO@ELTECOL.POL.LUBLIN.PL
tel: 551051 ext. 277, 271

Announcement

Now, we are pleased to announce the next ELMECO'96. This time we are also going to focus on topics which were the conference session titles. You can expect our *First Call* by July'95

Conference site was:
Dom Dziennikarza
ul. Małachowskiego 17, 24-120 Kazimierz Dolny
tel (0-831) 10-162, fax: (0-831) 10-165

ISBN 83-86333-01-4

Druk: Zakład Wydawniczo-Poligraficzny Politechniki Lubelskiej
20-950 Lublin, ul. Bernardyńska 13
Nakł. 120 egz., f. A4. Ark. wyd. 3. Ark. druk. 7,5. Zam 116/94

LIST OF CONTENTS

Iwo POLLO
Technical University of Lublin, Poland
Chair for Chemical Technology

Electrical Engineering and Environmental Plasma Chemistry

Introduction

For the history of sciences the past three centuries are a very important period. The modern world civilization started with the beginning of the connection between science and technnology. It is very interesting that the first discoveries on the start of new point of view on the nature and on the exploration of its mysteries were among others: the Boyle's "sceptical chemist's" declaration and the construction of the first electrostatic generator. The main problem of chemical investigation became to be the constitution of matter. During a long time the empirical data as well as the different ideas were compared and studied for to find the solution. Later one hundred years of the chemical science development has gone over the important way from the modern definition of the element given by Antoine Lavoisier and Dalton's atomic theory to the comprehension that the smallest chemical species consist of positively charged nucleus surrounding with a number of much slighter particles being elementary negative charge carriers. As the result of electron's rotation atoms and molecules are electromagnetic systems, every one has its own unrepeatable magnetic moment as well as electric properties. These circumstances justify the thesis about electric mechanism or electromagnetic one of chemical processes. Electrochemistry and magneto-chemistry are now the large branches of chemistry and the theory of chemical bounds could not develop without understanding of the electric field properties. Among four fundamental interactions: electromagnetic, strong, weak and gravitational one, only the first of them is really important for chemical bounds.

The most developed branch of chemical technology using directly electrical current to realize reactions on a commercial scale is the electrochemistry of water solutions. Much older seems to be the electrochemistry of gases: reactions in the gas phase caused by the electrical current have been studied from the XVIII century. For this purpose the mentioned electrostatic generator has been used. The first investigators working on this problem were rev. Joseph Priestley and sir Henry Cavendish. The early executed researches on the action of the electric spark on air permitted to draw the important conclusions concerning the constitution of air and to distinguish different kinds of gases (known today as nitrogen, hydrogen, oxygen, nitrogen oxides). Cavendish reported even about the appearing in his experiments of an inert fraction in air. Really the noble gases have been discovered a hundred years after his experiments.

In the beginning of XIX century an important form of electrical discharge - the arc - was discovered. A half century later the Faraday's works enabled the construction of the of high voltage sources. Using these devices one obtained some new form of discharges: silent discharge, glow, corona. It's interesting that the knowledge about each form of electric current flow through the gas formed the ground for important discoveries in the modern science and technology. X - ray, one synthesis, fluorescent lamp, electrical precipitator, electron tube - these are only some example from different branches of the knowledge.

Although chemical processes in electrical discharge have been continuously investigated for more than two centuries, only 70 years ago Langmuir proposed the name "plasma" for the ionized gas, where the elementary processes cause much of interesting physical and chemical phenomena. The possibility of creation of the ionized high temperature gas stream exists forty years . This invention was fruitful for the fast development of plasma chemistry. Now the realization of chemical reactions in the ionized gas is the object of research - beside chemistry - also of physics and the scientists working on the field of electrical engineering. A large number of periodic symposiums are organized now where the papers connected to plasma chemistry are referred. The most important meetings are: International Symposiums on Plasma Chemistry organized by International Union of Pure and Applied Chemistry, the European and World Congresses on Phenomena in Ionized Gases, world and regional Congresses on Ozone Science and Technology, conferences on Application of Electrical Discharges, Low Temperature High Pressure Plasma Chemistry Symposiums. The plasma sections are also present among topics of more general scientific and technical reunions. On all of them the reactions important for environmental protection are discussed. Now the organizers of ELMECO symposium have chosen the application of electromagnetic devices and processes in the environmental engineering as the main subject of presentation. Therefore the significant number of chemist - technologists are present with the communications concerning different applications of electrical discharge for environmentally important chemical processes.

Electrical discharges and chemical processes

The up-to-date researches on the chemical processes activated by electric discharge are realized using either the plasma stream with the high gas' temperature (order of kilokelvin or more) or in the so called cold plasma. According to the accepted custom the plasma stream as reaction environment is known as isotherm or equilibrium plasma. Really, there are no fully isotherm plasmas, it is only possible to discuss the local equilibrium. From the other side the obtained quantity of products in these conditions corresponds commonly with the equilibrium concentrations. The cold or rather non - plasma is formed either in the low pressure discharges or in special types of discharge like silent (barrier) or corona ones.

Really, the distinction between isotherm and non - equilibrium reaction conditions is not simple. Par example it is not clear, if the high frequency discharges or microwave ones can be treated in all cases on the base of the same thermodynamic presumption.

The indicated theoretical difficulties cause that plasma chemistry develops as an experimental science, only the obtained results permit to propose theories to prove to anticipate - always very carefully - the chemical properties of the investigated system.

From the practical point of view the inventions in plasma chemistry were used to realise the technologies important in environmental engineering almost from the beginning of researches on this field. I wanted here to present some problems of environmental plasma chemistry with reference to works realised in the chair for Chemical Technology in the Technical University of Lublin. First of all the problems of ozone synthesis will be presented.

OZONE AND ITS FORMATION IN SILENT DISCHARGE

The first - and for many years the only one - plasma chemical reaction realised on the larger as laboratory scale - is the ozone synthesis in the silent discharges. This process elaborated by Walter von Siemens in the year 1856 had from the beginning all distinctive marks of modern technology and additionally was connected to the environmental engineering. Siemens proposed to use the ozonizer as a source of the strong oxidizing agent for water treatment. In the next years this conception was proved as very useful. Particularly, the cholera pandemic, which expanded in the Europe, could be stopped owing to chlorine and ozone application for the municipal water treatment. Then the ozone use for this purpose increased and decreased in the dependence on the relative electrical energy costs. In the second half of XX century the importance of ozone became to rise and now this substance is one of the most important product for a large number of applications. The ozonation in the course of water treatment is an important up-to-day technology. The use of ozone assures the disinfection of water, but also the elimination of several heavy metals, as well of the bad taste, odor, strange colors.

The relatively new application of ozone is its using for waste water cleaning. There are several substances, par example aromatic or unsaturated organic compounds, which can be removed from the water phase only by the action of strongest oxidizing agents. The advantage of ozone is that between oxidation products there are no toxic or undesirable individuals. Ozone assures the oxidation to water and carbon dioxide. The only one condition is to use the sufficiently high ozone dose. This circumstance causes, that often ozone use is too expensive. The developing of ozonizers and electrical supply systems assured in the past the decreasing of energy losses and increasing of ozone yield. Now, every year the ozone production and the capacity of industrial installations increase.

Although the investigations on the ozone properties, conditions of its obtaining and possible area of the application are continuing during 150 years, the large number of problems does not find the satisfying solution. In the few past years the discussion on ozone appearance in the atmosphere has intensified. There is considered ozone in troposphere as a danger pollutant as well as ozone in the stratosphere as a protector against UV radiation. The diminishing of ozone concentration in higher atmosphere layers is known as an ozone hole. Particularly the so named Antarctic hole has been investigated using the most modern technicques.

The ozone production on an industrial scale has several particular difficulties. The chemical engineering needs for design of the process some physic - chemical numeric data. The most important are: equilibrium constant, rate constant, reaction order, activation energy, so called pre - exponential factor determining the rate - temperature dependence, reaction enthalpy, Gibbs' function values. For the processes in non - equilibrium plasmas these data are not known. The summary reaction:

$$3\,O_2 = 2\,O_3$$

does not represent faithfully the mechanism and real channels of the process. The calculated equilibrium constant is very small in the large interval of the temperature. Taken into account the thermodynamics of this summary relation one comes to the conclusion that only traces of ozone formed from oxygen or air should be expected. To eliminate theoretical difficulties one proposed the more complicated mechanism of ozone formation:

$$O_2 + e = 2\,O + e$$

$$O + O_2 = O_3^*$$

$$O_3^* + M = O_3 + M$$

In this reactions "e" means electron, "O_3^*" exited ozone molecule, "M" is a "third body" needed for carrying away the non - balanced quantities of energy. The reactions explaining the ozone formation should be complete by the other ones concerning ozone decomposition in the discharge. The most simple reaction can be presented as follows:

$$O_3 + e = O_2 + O + e$$

The presented schema explains good the possibility of obtaining "overquilibrium" ozone concentration, but does not give any numeric values for its calculation. There are no universal data for reactions with the presence of electrons. Also electrons' concentration in the discharge is not known. Additionally there was proposed another, complementary channel for ozone formation:

$$O_2 + e = O_2^V + e$$

$$O_2^V + 2\,O_2 = 2\,O_3$$

or

$$2\,O_2^V + O_2 = 2\,O_3$$

or

$$3O_2^V = 2\,O_3$$

In this mechanism "O_2^V" is a vibrationally exited oxygen molecule. The produced ozone can rest on an exited state and the recombination goes on after the collision with the third particle like in the first mechanism.

This channel is kinetically less possible, as well it preview the collision of three molecules, but some researchers suggest, that approximately 10% of ozone can be formed as the result of the appearing of exited oxygen molecules.

From the physical point of view the electron avalanches and streamers formation as well as the time of their duration should be important. Kogelschatz and some other scientists estimated the time of three stages of the total ozone formation process:

The first stage is the collision of oxygen with electrons in the electron avalanches in the microdischarges. Its duration is of the order of nanoseconds.

The second stage is the chemical process of oxygen atoms and oxygen molecules in the gas volume according to the microdischarge space. The duration is of the order of microseconds.

The third stage is the diffusion of formed ozone and equalization of ozone concentration. The duration of this stage is of the order of miliseconds.

Very important for the final result of ozone production are: the number of microdischarge in the discharge gap and the phenomena inside avalanche channels. In the agreement with accepted opinions the registered current depends on the quantity of microdischarges. The attempts to intensify the discharge over a limit of microdischarge concentration can transform the silent discharge into the spark or arc accompanying by the destruction of dielectrics. The elaborated theory indicates also, that for the rising of ozone concentration the increasing of current density over some kiloherz is purposeless. The time of the order milisecond is indispensable to assure the ozone's diffusion behind microdischarge channel and to diminish its local concentration. It was earlier shown, that electrons can destroy ozone with the rate proportional to its volume density. The synthesis goes on with the best yield, when temporally ozone is absent in the miocrodischarge channel.

The knowing this circumstances caused the not ended till now investigations on the microdischarge properties and namely there are searched the following data: the time of microdischarge duration, the area occupying the electrode surface, the geometry of electron avalanches and of the streamers, electron density in the microdischarge, its distribution in the channel, the distribution of electron energy, the temperature of ions and of neutrals particles. Not all of named discharge properties are known till now. Additionally there should be useful to have the information about thermodynamics and kinetics of processes with the participation of charged species. This problem for the microdischarge did not find also any final solution, since the obtained optical signals are very weak and their duration is short.

The phenomenology of ozone synthesis has been the topic of several studies during a very long time. The results were only partially published, the enterprises producing commercial ozonizers do not publish the data important for its design.

Then the problem of limit ozone concentrations obtained in the silent discharges is complicated enough. It depends on a large number of factors like:

- the inlet gas quality (mainly used: air, oxygen, air reached by oxygen),
- the discharge gap size,
- the dielectric thickness,
- the frequency and form of electrical current,
- the contain of impurities, at first of water vapour in the inlet gas,
- the material of electrode surface,
- the presence of adsorbed substances on the surface of electrode or dielectrics,
- the physical state of electrode surface,
- the dielectric properties of non - conducted barrier,
- the chemical and physical properties of the dielectrics
- the temperature of cooling water,
- the conditions of heat transfer in the ozonizer,
- the inlet gas temperature,
- the temperature inside the discharge gap,
- the presence of homogeneous catalyst in the inlet gas,
- the presence of heterogeneous catalyst inside discharge gap volume,
- the parallel forming of other forms of discharges like surface one,

- the influencing of the other external factors like UV radiation,
- the additional presence of elements causing the changes of discharge form like so named a mesh electrode located under the dielectric layer.

The same list of factors determines the rate constant values.

The energy balance of installations for ozone production is a complicated task as well there are no level for to estimate the theoretical level. Taking into account only the reaction enthalpy of summary reaction, the energetic yield of ozone production in the ozonizer does not exceed 10%. Then the works on energy balance for ozonizers and connected systems are of a large importance. The first published papers concerning the ozonizers' energy balances have origin in our laboratory.

The design of devices for current supply is an other problem developed in Technical University of Lublin by the Prof. Janowski's group.

The most part of industrial ozonizers use the silent discharge. The other low temperature high pressure plasma enviroments were also proved for this aim. The interesting form of discharges seems to be the corona discharge supplied by direct current or by alternative one.

CORONA DISCHARGES AND ENVIRONMENTAL CHEMISTRY

D.c. corona discharge devices commonly are used as electrostatic precipitators. The low energy of the discharge and the possibility of spark formation causes that this form of discharge cannot be applicated to realise controlled chemical processes. Introduction of the dielectric barrier stabilize the discharge and the supplying by a.c. current enable the obtaining higher energy densities. This form of discharge (called also semi - corona discharge) can be treated as the alternative ozone sources.

The concentration of ozone obtained in corona discharge is less, than in silent one. There are other advantages making corona devices interesting for practical use. The construction is more simple and more shock - resistant. An important property is much larger distance between electrodes. This enables the filling of the discharge gap with catalyst like in the work of Prof. Schmidt-Szałowski's group. From the point of view of science the details concerning the structure of semi - corona discharge are not known as well as all factors connected to the chemical reaction. This opens the research possibilities.

The relatively new form of corona discharge is pulse corona. There were executed some works confirming the possibility to use it to clean gas processes. Particularly it is possible to eliminate nitrogen oxides, sulphur oxides as well as a number of organic compounds from different waste gases.

SUMMARY

Up-to date interdisciplinary problems gain on the importance in the science. Particularly they are developing in the environmental sciences. And the environment protection is now and will be in the next years the main problem of the civilisation.

In the paper the topics being object of research in our laboratory have been indicated. The extended discussion concerns ozone formation in the plasma of electrical silent discharges. But also some other processes in different forms of discharge must be taken into account. This confirms the necessity of nearing two branches: electrical engineering and chemical technology. Really, electrical science and chemistry cannot be separated. For the future, it will be necessary to make the co-operation among engineers of different branches more fruitful.

A.Czernichowski (1), A. Ranaivosoloarimanana (1), T. Janowski (2), H. D. Stryczewska (2), M. Cojan (3), A.A. Fridman (4)
(1) Orleans University, GREMI, 45067 Orleans cedex 02, France
(2) Lublin Technical University, 20-618 Lublin, Poland
(3) Technical University, 6600 Iasi, Romania
(4) Kurchatov Institute, 123182 Moscow, Russia

PLASMA-CHEMICAL PROCESSING OF CO_2 IN A GLIDING ARC REACTOR SUPPLIED AT 50 OR 150 Hz

Abstract

An endothermal test-reaction of pure carbon monoxide decomposition $CO_2 = CO + 1/2\ O_2$ in two non-equilibrium plasma reactors at atmospheric pressure is carried out in order to determine an influence of the power supply frequency on energetic efficiency of the reaction. A simple two-electrode laboratory-scale reactor based on the principle of gliding arcs is powered up to 300 W via two different high voltage suppliers (50 or 150 Hz), while electrode's material and geometry remain unchanged. Also the gas flow-rates range is the same (12 - 25 l/min). The set-up parameters as well as the off-gas composition are carefully determined via electrical sensors, calorimetry and gas chromatography. More powerful 50/150 Hz supply (up to 2 kW) and another "3+1"-electrode reactor at much higher gas flow rate are also tested for pure CO_2 dissociation.

Introduction

Emission of carbon dioxide due to combustion of fossil fuels and iron making industry are responsible for about 60% of the man made greenhouse effect. A large set from several technological options [1] (the references in this paper are given only as an example) for controlling this emission is:

A. a direct conversion of CO_2 into organic compounds utilized as raw materials for chemical industries and secondary energy, like:
   1. methanol: $CO_2 + 3\ H_2 = CH_3OH + H_2O$,
   2. methane: $CO_2 + 4\ H_2 = CH_4 + 2\ H_2O$,
   3. synthetic crude oil (syncrude) via direct Fischer - Tropsch reaction:
      $n\ (CO_2 + 3\ H_2) = (CH_2)_n + 2n\ H_2O$,
   4. electrochemical reduction of CO_2 to organics,
   5. photo-synthesis: $CO_2 + H_2O = HCOOH + 0.5\ O_2$ which had already been achieved artificially in XIX century, or

B. CO_2 transformation into CO via:

6. gasification of carbonaceous matter: $CO_2 + C = 2\ CO$,
7. methane reforming: $CO_2 + CH_4 = 2\ CO + 2\ H_2$,
8. direct dissociation: $CO_2 = CO + 0.5\ O_2$,
9. electro-catalytic reduction in water,

and then a CO-involved chemistry like:

10. transforming into hydrogen, the futuristic clean fuel, via so-called shift reaction with steam: $CO + 2\ H_2 = CO_2 + H_2$,
11. methanol production: $CO + 2\ H_2 = CH_3OH$,
12. syncrude production: $n\ (CO + 2\ H_2) = (CH_2)_n + n\ H_2O$.

Most of these processes are unfortunately endothermal ones. However, if necessary energy is produced via a CO_2-free way(e.g. using solar, hydro, wind, nuclear or biomass and reforestation processes), then the waste CO_2 can be considered rather as a carbon-contained raw material to make synthetic fuels! Although CO_2 molecules finally end up in the atmosphere they have been used twice and thus their global warming potential has been halved.

Direct CO_2 dissociation has been under examination since long years as source of CO for chemistry. It is also studied for other reasons, as it appears:

- in CO_2 lasers where CO production is an adverse side-process and where a transition from electric glow to arc discharge limits the power deposited in the glow discharge below the instability threshold,
- during modification of plastics (like polyethylene) via CO_2 plasma,
- during welding and/or arc cutting in CO_2 atmosphere, etc.

The conversion degree of CO_2 decomposition processes is rarely 100% and therefore they should be linked to an efficient CO separation process from gas products.

Thermal Dissociation

The Thermodynamics gives the standard enthalpy of CO_2 dissociation to CO and O_2 equal to 283 kJ/mol (or 2.93 eV/ molecule or 2.81 kWh per 1 kg of produced CO) at the standard condition (1 atm. 298 K). At this condition, only 10^{-16} part of initial CO_2 is dissociated into CO [2]. Therefore, one has to heat CO_2 to get more CO, for example (under atmospheric pressure) up to 1930 K to obtain 1% of initial pure CO_2 transformed into CO, or up to 2430 K or 3070 K to obtain 10% or 50%, respectively. It will ask for an extra energy to heat all gas, so that the Specific Energy Requirement (SER) necessary to obtain 1 kg of carbon monoxide will be rather 95 or 14.66 or 6.22 kWh, respectively for 1930, 2430 and 3070 K. Figure 1 presents the dissociation degree of CO_2 as well as the SER as a function of temperature for two pressures (1 atm and 100 Torr).

The theoretical SER minimum of 5.88 kWh/kg CO under atmospheric pressure is located at 3300 K which corresponds to the Specific Energy Input (SEI means the energy per 1 kg of initial CO_2) of 2.51 kWh/kg CO_2; at this temperature67% of the initial CO_2 should be transformed to the CO. One can imagine an "absolute quench" process in which all COP product is conserved (no reverse reaction); such process will cost 5.88 kWh/kg CO. However, at this temperature another product of CO_2 dissociation, molecular oxygen, will also be dissociated itself to the atomic form (17.1 mole O + 25.0 mole O_2 from 100 mole of initial

CO_2). An "ideal quench" can then be imagined: active O atoms attack the remaining CO_2 molecules to produce a supplementary amount of CO via a radicalary reaction: $CO_2 + O = CO + O_2$.

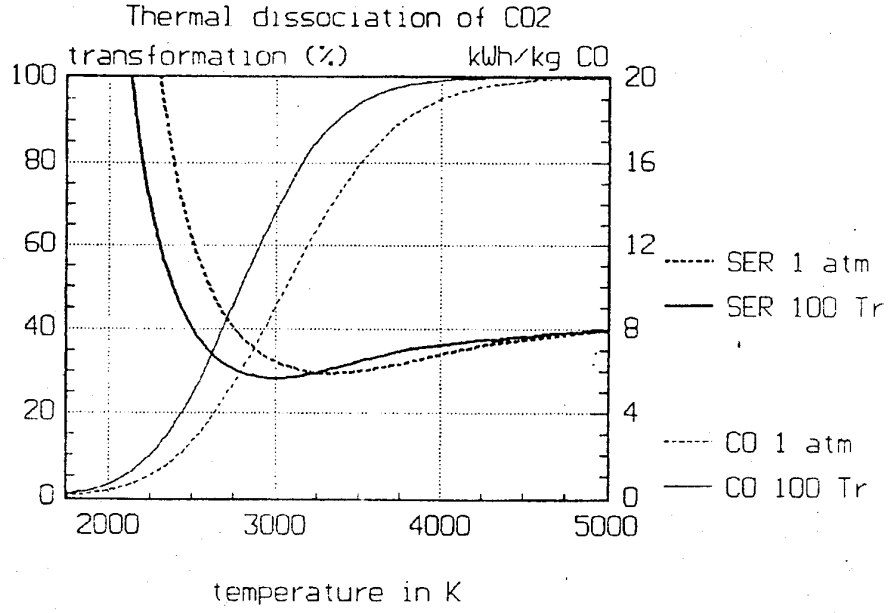

Fig. 1. Thermal dissociation degree of Carbon Dioxide (%) and Specific Energy Requirement (SER) necessary to obtain 1 kg of Carbon Monoxide as a function of temperature for two pressures (1 atm and 100 Torr) kept constant.

It means that to perform the CO_2 dissociation (case of an "absolute quench") one should spent about twice as much of energy than the standard one or, in other words, that the theoretical limit of energy efficiency of CO_2 dissociation in thermal equilibrium system is 48% at 1 atm (the energy efficiency means here the ratio of reaction enthalpy with respect to real energy spent in reactor).

This theoretical value may be lowered via heat exchange, but because of a reverse reaction of CO + O recombination into CO_2, the high temperature product must be quenched very quickly and therefore only limited heat exchange can be technically achieved.

Slightly lower minimal SER can be theoretically obtained at reduced pressures, for example 5.64 kWh/kg CO at 100 Torr and 3000 K (SEI = 2.43 kWh/kg CO_2) where the CO_2 dissociation reaches 68% and the theoretical limit of energy efficiency of CO_2 dissociation in thermal equilibrium system is 50%. A practical application of reduced pressures will ask however for an extra energy of mild-vacuum pumping.

As an example of the thermal dissociation, a membrane reactor system for thermal decomposition of CO_2 was recently proposed: an yttria-stabilized zirconia membrane plays there also a catalyst role. It was found that such a membrane reactor system may improve the final CO_2 conversion [3].

Electrically Assisted CO_2 Dissociation

The process of CO_2 decomposition has been investigated in practically all types of electrical discharges.

Generally conventional electric arcs or plasma torches generating a so called "thermal plasma" seem not to be adapted to gas processing. A molecular gas can not easily interact with a confined zone of very high energy. Moreover, under atmospheric or higher pressures, thermalization (which means a close-to-thermodynamic equilibrium state) at high temperatures of several kK are observed. In such conditions, the process of gas processing is first of all its expensive over-heating (complete thermal dissociation to atoms, ions and electrons) which must then be followed by rapid cooling (in order to quench the high temperature chemical equilibria).

In arc discharges [4] the process energy efficiency of 20 to 35% (with respect of those corresponding to thermal equilibrium mechanism) was obtained.

A pure Argon plasma-torch for CO_2 decomposition are described in [5]: in 5 kW atmospheric pressure reactor at CO_2/Ar molar ratio of 0.18, 0.40 or 0.65 (at the constant Ar flow-rate of 1.6 Nm^3/h) up to 26% conversion was observed: it is however difficult to extract the energy cost of the process from this publication. Almost the same approach was presented in [6] where CO_2 was also injected at the Argon jet of a classical 3 kW plasma torch in proportions up to CO_2/Ar = 0.15 and then quenched: 28 to 84% conversion was observed at the energy price (SER) of at least 70 kWh/kg of CO.

High energy efficiencies of CO_2 dissociation can be however obtained via non-equilibrium processes in non-thermal plasmas. Modelling of such processes (and generally endothermal or high energy activation barrier reactions) has been underlined by several authors; papers and reviews (like [7]) had been published since last decades in this particular field. However, in completely cold non-equilibrium systems (like corona or glow) where dissociation is mainly stimulated by electronic excitation, the theoretical limit of energy efficiency is about 30%, see [8] and [9].

Several types of close-to-atmospheric pressure non-equilibrium plasmas have been examined, like:

- glow discharge,
- radio-frequency (RF),
- high-voltage pulse (spark) discharge,
- corona,
- microwave plasma,
- silent (or dielectric barrier) discharge,
- ac ferroelectric pellet reactor.

However, the power of most of such non-equilibrium discharges is limited and/or their reactor structures are quite complicated and/or their power supply systems have quite low efficient energy transformation factors.

In non-equilibrium glow discharges [10] the energy efficiency was quite low (not more than 15%). This fact is connected with one of non-equilibrium mechanisms of dissociation via not so much effective excitation of electronic states of CO_2 molecule. In more recent work [11] a 86% decomposition of initially pure CO_2 was obtained in a glow discharge under 2 Torr (such a low pressure can not be acceptable from practical point of view) but no energy price was reported.

The energy efficiency of CO_2 dissociation through vibrational excitation of CO_2 molecules in non-thermal plasmas was theoretically anticipated quite early [12] and experimentally verified [13] in a 1 kW, 21 MHz discharge at low pressure (up to 3 Torr) where up to 80% CO_2 was dissociated for the relative plasma chemical efficiency of 30 - 40%. In another (?) RF discharge [14] this energy efficiency have not exceeded 60% because of too high energy input.

The CO_2 at 1 bar was dissociated using a spark discharge of modified commercial plug called "plasma jet igniter" [15]; the pulse period was 6 - 150 ms at pulls energy of only 12 to 100 mJ for CO_2 flow-rate of 1 to 10 cm^3/min. The CO_2 degree of dissociation reached 20% and the ratio of electrical energy input to chemical stored energy was not higher than 9%. Some recent results concerning a very low power pulse plasma applied for CO_2 decomposition under atmospheric pressure were described in [16]; up to 27% of CO_2 dissociation was observed but the minimum value of energy consumption was 66kWh/kg CO.

Stagnant air-CO_2 mixture (5%) has been treated in point-to-cylinder corona [17] where up to 24% conversion was observed; no energetics was done. Some experiments were also described in [18] with 3% flowing mixture in a point-to-plane reactor, but no dissociation rate nor energetics were reported.

Advantages of supersonic Very High Frequency (VHF) plasmatrons were underlined in several papers from Rusanov group (Russian Research Center, Kurchatov Institute) published since 1981, but these powerful reactors (up to 1MW), are quite complicated and perhaps too expensive for larger industrial applications. However, very high energy efficiency has been obtained in these non-equilibrium microwave discharges at lowered pressures. The first one [19] was realised in a laboratory scale device (2.45 GHz, 2 kW, 600 cm^3/s, 120 Torr) where the energy efficiency up to 80% has been obtained. The mechanism of the process was identified: a stimulation of the dissociation process by vibrational excitation of CO_2 molecules. The second stage was realised [20] in a pilot plant of 100 kW at 0.9 GHz where a super sonic (Mach 3) microwave plasmatron has been used and the energy efficiency up to 90% was observed for vibrational temperature of about 4 kK and translational one at only 100 K level (see also [21]). The high value of energy efficiency (up to 80%) has also been confirmed in a small industrial plant (0.9 GHz, 50 kW) in Grodno, Belarus [22].

Reduction of CO_2 by the Alternate-Current (AC) atmospheric pressure 40 W ferroelectric reactor was recently presented in [23] where only diluted H_2S, (10% in air) was used. The average decomposition rate to CO was 54% while the best energetic price was 30 kWh/kg CO.

Gliding arc

New way of plasma generation by formation of gliding electrical arc discharge has been developed in Orleans. At least two diverging electrodes are placed in a fast gas flow and in the flow direction. The discharges are organized between the electrodes and across the flow. The displacement of the discharge roots on electrodes prevents their erosion. The electrical energy is directly and totally transferred to the gas. All gas or vapour like Ar, N_2, O_2, H_2, CO_2, CO, H_2S, CH_4, SO_2, N_2O, other hydrocarbons, chloroform, freons, steam, air, and some of their mixtures can be directly processed at any inlet temperature and 0.1 - 5 atm pressures at negligible pressure drop. Dusty and/or misty fluids are accepted.

Quite big plasma volume at relatively low energy density is out of the thermodynamic equilibrium. A transient characteristic of the discharge is similar to the glow discharge characteristics but it is difficult to define what "the glow discharge is" and what "the low current arc" is when the electric energy is put across the fast and turbulent gas flow and when the discharge/arc roots move rapidly along the electrodes. So we use both terms: discharge or arc and call such device as GlidArc.

The discharge starts at the shortest distance between the electrodes and within a very short time there is formation of a low resistance plasma; the voltage falls. The small plasma volume is then dragged by the gas flow at a speed about 10 m/s, and both the length and

voltage of the arc column increase together with the distance between the electrodes. The plasma in this stage is close to the thermodynamic equilibrium because the electrical power delivered by the generator is sufficient to compensate energy losses by thermal conduction. Then a striking phenomenon occurs: a transition to a step-wise ionisation mechanism linked to a sudden increase in arc length (up to four times) clearly visible on pictures taken with a high speed camera, see [24]. In such way the electrical energy is directly used to produce a non-equilibrium and very reactive medium allowing efficient gas processing so that up to 45% of this energy may be directly absorbed in an endothermic reaction. Therefore the main innovative aspect of the GlidArc process is certainly the way in which the chemical reactions are activated via powerful electrical discharges under near-to-atmospheric pressures.

Some applications of the GlidArc were tested in a laboratory and close-to industrial scale reactors and already disclosed, see [25]:

- flame overheating (electro-burner),
- air cleaning from volatile hazardous compounds,
- complete or partial beneficiation of concentrated H_2S, or $H_2S + CO_2$ mixtures,
- flue gas SO_2 reduction to elementary sulphur,
- natural gas conversion to the syngas ($H_2 + CO$).

New applications if GlidArc are recently tested, like:

- cleaning of flue gas from the combustion of explosives [26],
- combustion of very lean methane-air mixtures [27],
- oxidation of chloroform vapours [28],
- steam overheating [29],
- upgrading oxidation of N_2O to NO_x [30],
- dehalogenation of $CHCl_3$, CF_2Cl_2 , $CFCl_3$ [31],
- activation of organic fibres [32].

The GlidArc technology development asks us now for a simple chemical system testing in order to see how some of its operational parameters can influence efficiency of plasma processing. The CO_2 dissociation has been chosen to examine an eventual influence of the electrical power supplier frequency for the same plasma reactor and other fixed parameters. Other tests where performed in another reactor for much higher gas flow-rates and supplied by more powerful special hybrid generator. The experiments should give us a comparison of our GlidArc technology results to other CO_2 decomposition tests from the literature.

Experiments

As schematically shown on Fig. 2, two diverging (with respect to each other) steel electrodes (0.8 mm thick, 10 cm length) are placed in a small flat reactor (A) in a relatively fast CO_2 flow and in the flow direction. Gliding discharges are produced between the electrodes and across the gas (12 to 30 Nl/min) formed by a 4 mm nozzle. They start at the spot where the distance between the electrodes is the shortest (about 1 mm) and spread by gliding progressively along the electrodes in the direction of flow until they disappear after a certain path (about 7 cm); at that stage the arc length is about 6.5 cm. The electrical discharges then immediately reform at the initial spot.

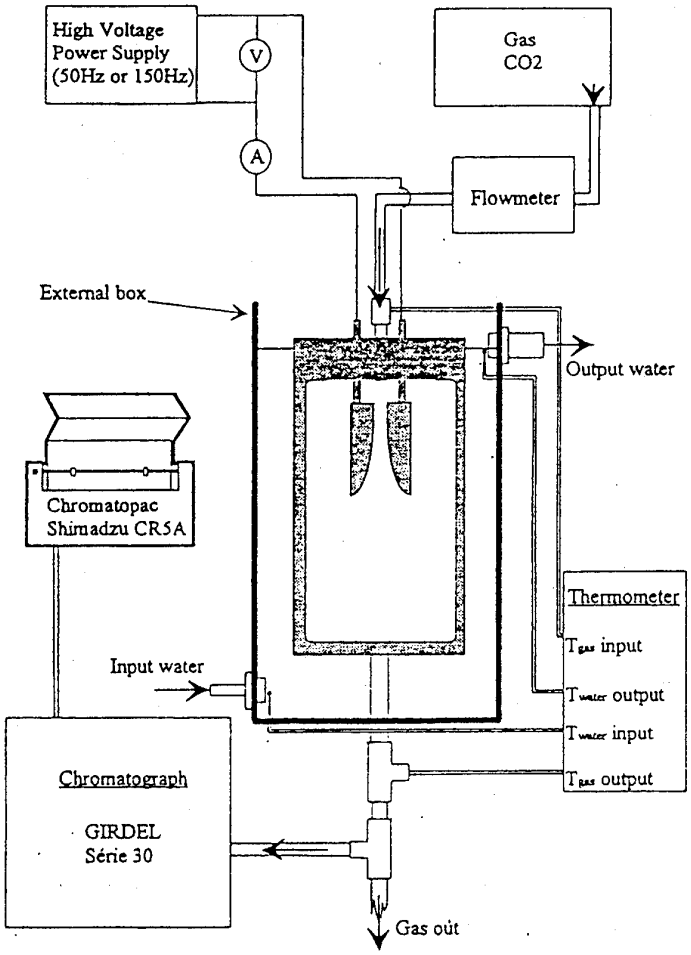

Fig. 2. Small GlidArc flat reactor (A) and some of its environment for CO_2 dissociation experiments.

The glass-metal reactor of a parallelepiped form (8.5 cm wide) of 1.2 l volume was plunged in a water calorimeter. Four thermometers allowed the precise temperature measurements (water input and output, gas input and output). Water flow-rate was constant (300 ml/min) and its temperature increase never exceeded 45 deg. C. The gas entered reactor at ambient temperature and at atmospheric pressure. Conducting walls of the reactor enabled the efficient gas product cooling so that the gas was never hotter than 70 deg. C at the reactor exit. The calorimeter was carefully calibrated via Joule effect; the accuracy of dissipated power is 5% for the power range out of plasma experiments. The entry gas flow-rate was precisely measured by a mass flow-meter so the Specific Energy Input (SEI) was carefully measured.

The exit was analysed "on line" via gas chromatography (for CO and O_2 content) so that the SER was precisely determined for all experiments.

Two High Voltage AC single-phase power suppliers were used for this reactor. The both generators were powered via primary regulated auto-transformer so that the power dissipated in the reactor could be easily controlled:

a. 50 Hz power supply is a classical neon transformer with an additional relatively self-inductance inserted in order to adjust the circuit impedance;

b. 150 Hz power supply is a special construction called magnetic frequency tripler in which one uses a three phase 50 Hz output of a self transformer to obtain, with appropriate connections, a single phase high voltage [33].

Two power suppliers have nearly the same circuit impedance of 20 kOhm and the same max. open circuit voltage of 4 kV necessary for the GlidArc self-ignition. After the ignition the arc could be easily limited in current in the range of 0.15 to 0.5 A. The power dissipated in the reactor (50 to 250 W) depended also on the gas flow-rate due to coupling of the gas turbulence and specific electric field of the discharge. Visibly, the gliding discharge at 150 Hz seemed more diffuse than those at 50 Hz. Also, for higher CO_2 flow-rates we observed more diffuse and more turbulent and filamentary like discharge while at lower ones a close-to-arc tendency was observed.

The power factor of both 50 and 150 Hz transformers (not optimized) was rather poor, about 30% , but the net power dissipated in the Reactor A was always carefully measured as a running parameter of our experiments.

Another cylindrical reactor (B) for CO_2 processing was almost the same as used for flue gas cleaning [26]: only one section among six serial mounted sections was used. The section was composed of a 80 mm in. dia. pyrex tube (500 mm long) in which 3 knife shaped steel electrodes are put around the tube axis. The electrode gap is starting at 5 mm (ignition) to become about 7 cm at the electrode top (discharge disappearance). However, instead of the discharge self-ignition of a three phase high voltage structure used before (each electrode connected to one output of a high voltage and high inductive 3-phase 50 Hz transformer), we use now a new proprietary structure of a medium voltage low inductive 3-phase 50 Hz transformer connected to a single phase high voltage (but very low power) special 150 Hz transformer [34], [35], (see Fig. 3). In such way one can obtain a good matching between electrical characteristics of the gliding arcs and the power supplier; it gives us a quite high po wer factor of about 0.8 which is close to an industrial requirement.

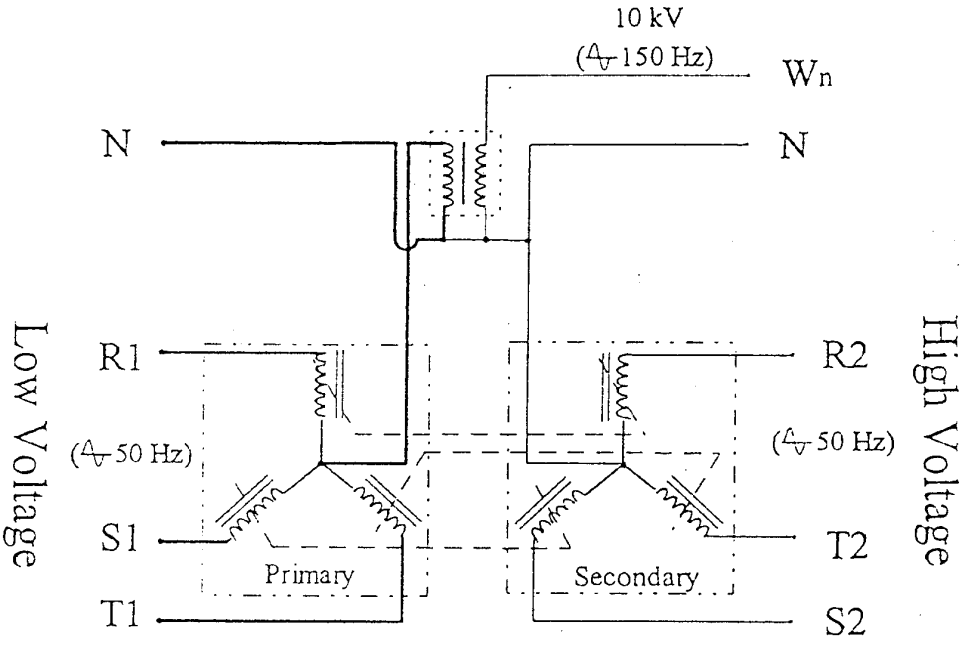

Fig. 3. Principle of 50/150 Hz power supply for 3+1 electrode GlidArc structure.

Results

Small Reactor A - 50 Hz

Three sets of experiments are performed at the input CO_2 flow-rate of 13, 15 and 20 Nl/min in the input power range of 53 to 232 W. The SEI of 17 runs ranged between 0.035 and 0.134 kWh/kg CO_2 which corresponds to an average gas temperature in the reactor between 440 and 770 K. As a result of such a low energy input, only 0.4 to 1.6 % of CO_2 was transformed to carbon oxide.

From the point of view of the energetic price of 1 kg of CO production, the results ranged between 9.5 and 16 kWh. the best result was obtained at 102 W and 20 Nl/min while at the low input CO_2 flow-rate of 13 Nl/min, we noticed the worst one at 54 W. Figure 4 presents the results of two sets of runs for two flow-rates.

Small Reactor A - 150 Hz

Almost the same ranges of the input CO_2 flow-rate of 12, 20, 25 and 30 Nl/min and the input power of 93 to 250 W were experimented. The SEI of 19 runs ranged between 0.032 and 0.161 kWh/kg CO_2 which corresponds to an average gas temperature in the reactor between 430 and 850 K. The dissociation degree ranged as before.

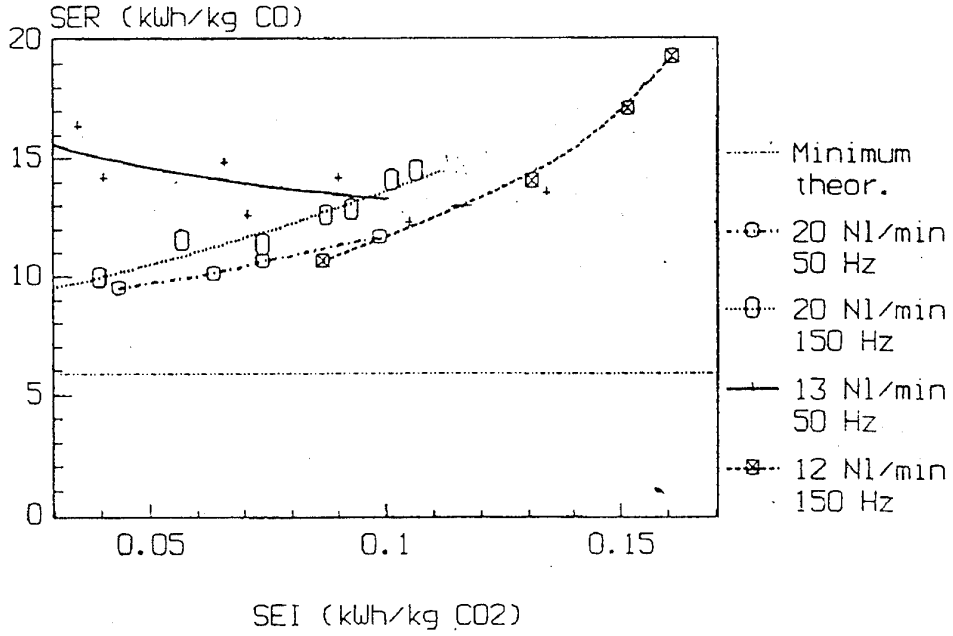

Fig. 4. Specific Energy Requirement SER) to produce 1 kg of Carbon Monoxide from pure CO_2 in the Reactor A powered at 50 or 150 Hz as a function of the Specific Energy Input (SEI) for two input gas flow-rates.

The best SER was 7.6 kWh/kg CO for 205 W and 30 Nl/min and the worst one (19 kWh/kg CO) belonged to 12 Nl/min and 228 W. Figure 5 presents the results of four sets of runs for different flow-rates and SEIs.

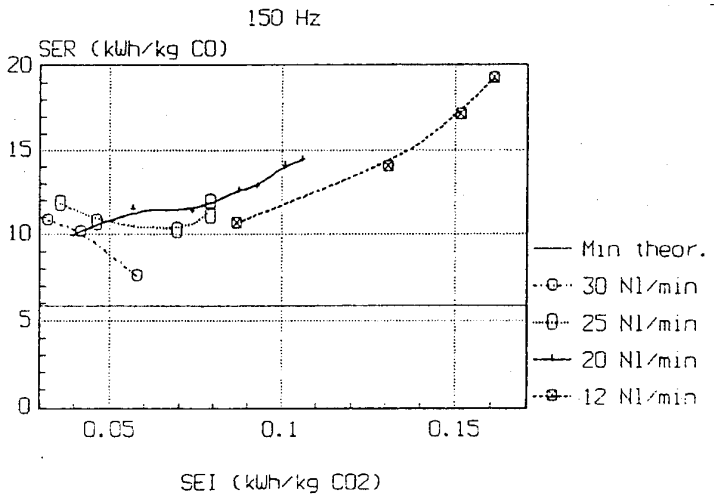

Fig. 5. Specific Energy Requirement (SER) to produce 1 kg of Carbon Monoxide from pure CO_2 in the Reactor A powered at 150 Hz as a function of the Specific Energy Input (SEI) for different input gas flow-rates.

Large Reactor B

Much higher CO_2 flow-rates were processed (up to 84 Nl/min) at higher power level of 1.0 to 1.6 kW. The electric power was however measured only at the input of the 50/150 Hz transformer so that the real power of the reactor could only be evaluated (about 80% of the measured one). As in the case of Reactor A, this reactor was not thermally isolated (we use other reactors where a partial energy recycling can be performed).

Six experimental sets (total 29 runs) were performed for pure CO_2 and in presence of water vapour or other gases (air, He, Ar, H_2 or N_2 separately). The CO concentration in products ranged from 0.5 to 3.4 vol. % corresponding to the transformation degree of CO_2 to CO from 0.6 to 3.7 %.

The best SER that we observed for pure CO_2 was 12 kWh/kg CO for 84 Nl/min entering CO_2 flow-rate and 1.04 kW which gives SEI = 0.105 kWh/kg CO_2 (it would correspond to an average temperature of 680 K). Figure 6 presents experimental data of this set. The same Fig. 6 presents also four runs which were made in presence of quite a high amount of water vapour (4.3 to 5.5 vol. %) for the SEI between 0.20 and 0.33 kWh/kg CO_2.

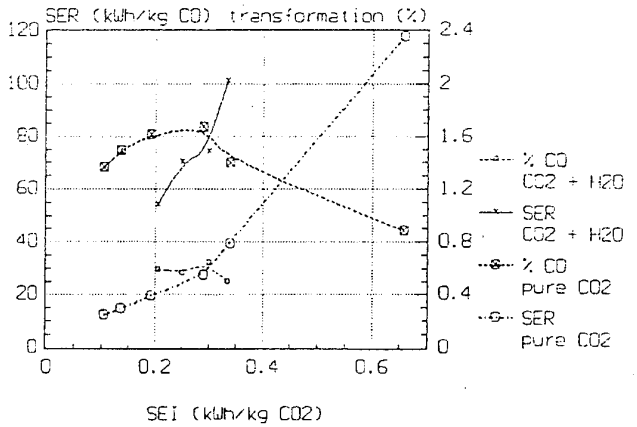

Fig. 6. Specific Energy Requirement (SER) to produce 1 kg of Carbon Monoxide from pure CO_2 or from a mixture of CO_2 with water vapour (4.3 to 5.5 vol. %) and corresponding

transformation degree to CO (%) in 3+1 electrodes GlidArc Reactor B as a function of the Specific energy Input (SEI).

A neutral gas addition to the main CO_2 stream (He, Ar, or N_2 at the concentrations up to 14, 21 or 17%, respectively) was examined in order to see an influence on both CO concentration in products and SER values. The air addition (up to 8%) was also examined in order to see an influence of the reverse reaction $CO + 0.5\ O_2 = CO_2$ on the amount of the carbon oxide in the exit product (see Fig. 7).

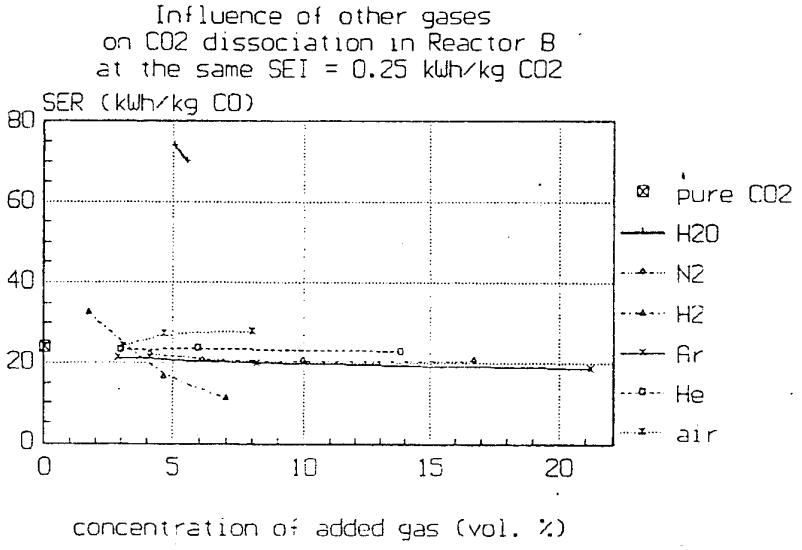

Fig. 7. Specific Energy Requirement (SER) to produce 1 kg of Carbon Monoxide from CO_2 rich gas mixture with water vapour or other gases (air, He, Ar, H_2 or N_2); the runs were performed in Reactor B at almost the same entry gas flow-rate and the same Specific Energy Input (SEI) of 0.25 kWh/kg CO_2

Discussion

1. One should underline the very low Specific Energy Input for all experiments, corresponding to quite low average gas temperatures. Evidently, a local temperature in the discharge filament is much higher (if one can really talk about temperatures in such a non-equilibrium discharge ...). For these low-SEI conditions we observe however quite good SER values ranged between 10 and 15 kWh/ kg CO.
2. No clear conclusion can be done when comparing 50 and 150 Hz power supplying (Fig. 4); the frequency of 50 Hz seems more efficient for low gas flow-rate while the 150 Hz one is better for higher flow-rate. This point should be clarified using a larger range of frequencies.
3. The price of CO produced at growing SEI (when other parameters are kept constant) increase as well. However this general tendency is not observed for 150 Hz at higher gas flow-rates (Fig. 5), especially for 30 Nl/min where we have obtained very good SER value of 7.6 kWh/kg CO at SEI = 0.058 kWh/kg CO_2 (which corresponds to the average temperature of only 520 K! It means that 37% of input electric energy was used for dissociation of CO_2 molecules. The tendancy of the curve let us think that lower SER values can even be obtained for slightly higher SEIs.

4. Almost the same results have been obtained in Reactor B for much higher CO_2 flow-rates where the best SER value is close 12 kWh/kg CO (or rather around 10 kWh/kg CO when taking into account a net energy injected to the reactor).
5. The air addition (up to 8%, see Fig. 7) has rather limited effect: an additional amount of oxygen in products makes the reverse reaction $CO + 0.5\ O_2 = CO_2$ easier, probably close to the discharge zone (CO molecule is too strongly build to be after-burned in a post-plasma region).
6. The results presented in Figs. 6 and 7 show highly destructive action of water vapour to the process (much lower CO concentractions in products and much higher SER values). It is certainly linked to the radical OH produced in the plasma via H_2O decomposition.
7. A neutral gas added to the main CO_2 stream (He, Ar or N_2) has shown no significant influence on CO concentration in products nor difference in SER values, see Fig. 7. A small lowering of SER values can be accounted to a dilution effect (see Fig. 1 where smaller partial pressure of CO_2 gives better SER).
8. Hydrogen addition to the CO_2 should artificially increase the CO concentration in product via classical reverse shift reaction $CO_2 + H_2 = CO + H_2O$. It is true for H_2 initial concentration greater than 4% (see Fig. 7). The reaction still works for lower H_2 concentration, but the destructive action of H_2O in product prevails.

Conclusion

The inexpensive and very simple gliding electric discharges are capable to dissociate carbon dioxide to CO. The use of such discharge brings to this process an easily controllable energy without corrosion or errosion of electrodes in presence of active oxygen.

Specific energy consumption observed in this quite cold plasma are relatively low (less than 10 kWh/kg CO) as compared to other results found in literature. These values can probably be lowered when using a higher frequency power supplier at higher gas flow-rates. Moisture in entering CO_2 should be avoided as it considerably lowers the process performance (such effect has been recently observed during the N_2O to NO_x beneficiation [31], too).

The present results may be helpful for further development of the powerful electric generators to supply full industrial scale GlidArc reactors. The laboratory scale non-catalytic methane/CO_2 reforming [37] as well as the pilot scale processing of a sour gas containing 20% H_2S + 75% CO_2 [38] are also concerned because the CO_2 decomposition to CO and active oxygen in situ production plays there an important role.

References

1. K. BLOK, W.C. TURKENBURG, C. HENDRIKS, M. STEINBERG (editors), Proc. of the First Int. Conf. on Carbon Dioxide Removal, Amsterdam, 4-6.03.1992, Pergamon Press, 826 pp
2. G.DELUC, M.F. ELCHINGER, B. PATERYON, ADEP, Universit de Limoges, LCMTS, Equipe Plasma Lasers Mat riaux, 1993
3. N.ITOH, C.M.A. SANCHEZ, X. WEI-CHUN, K. HARAYA, M. HONGO, J. of Membrane Sci., vol. 77, 245 (1993)
4. Yu. P. BUTYLKIN, A.A. GIERENKO, A.A. LEVITSKI, L.S. POLAK, N.M. RYTOVA, D.I. SLOVETSKII, Khim. Vys. Energ., vol. 13, 545 (1979)
5. A.HUCZKO, A.SZYMAŃSKI, Plasma Chem. and Plasma Processing, vol.4, 59 (1984)

6. H.SEKIGUCHI, T.HONDA, A.KANZAWA, 8th Int. Symp. on Plasma Chemistry, Tokyo, 31.08-04.09.1987, p. 713
7. A.A. FRIDMAN, V.D. RUSANOV, Pure and Appl. Chem., vol. 66, 1267 (1994)
8. V.D. RUSANOV, A.A. FRIDMAN, Fizika Khimicheski Aktivnoi Plazmy, Nauka, Moscow, 1984, 415 pp.
9. S.A.NESTER, B.V. POTAPKIN, A.A. LEVICKIJ, V.D. RUSANOV, B.G. TRUSOV, A.A. FRIDMAN, Kinetiki-Statisticheskie Modelirovanie Khimicheskih Reakcij v Gazovom Razriade. Gos. Kom. Ispol. Atom. Ener. SSSR, Moscow, 1988, 222 pp
10. K.K. CORVIN, S.J. CORIGAN, J. Chem. Phys. vol. 50, 2570 (1969)
11. K.TANAKA, H. MIYOSHI, 9th Int. Symp. on Plasma Chemistry, Pugnochuso, Italy, 4-8.09.1989, p. 774
12. V.A. LEGASOV, V.D. RUSANOV. A.A. FRIDMAN, G.V. SHOLIN, 3rd Int. Symp. on Plasma Chemistry, Limoges, France, 13-19. 07. 1977, paper g.5.18
13. B.I. PATRUSHEV, G.V. RYKUNOV, A.M. SPECTOR, 3rd Int. Symp. on Plasma Chemistry, Limoges, France, 13-19. 07. 1977, paper g.2.18
14. V.A. LEGASOV, V.D. RUSANOV, A.A. FRIDMAN, V.G. JIVOTOV, B.I. PETRUSHEV, A.M. SPECTOR, G.V. RYKUNOV, E.G. KRASHENINNIKOV et. all. Dokl. Akad. Nauk SSSR, vol. 238, p. 66 (1978)
15. H.R. WEISS 7th Int. Symp. on Plasma Chemistry, Eindhoven, Netherlands, 1-5.07.1985, p. 383
16. A. RESZTAK, A. SZYMAŃSKI, 11th INt. Symp. on Plasma Chemistry, Loughborough, England, 22-27.08.1993, p. 650
17. M. HIGASHI, M. SUGAYA, K. UEKI, K. FUJII, 7th Int. Symp. on Plasma Chemistry, Eindhoven, Netherlands, 1-5.07.1985, p. 366
18. N. BOUKHALFA, A. GOLGMAN, M. GOLDMAN, R.S. SIGMOND, 8th Int. Symp. on Plasma Chemistry, Tokyo, 31.08-04.09.1987, p. 787
19. V.G. JIVOTOV, V.D. RUSANOV, E.G. KRASENINNIKOV, YU. P. BUTYLKIN et all., J. Tech. Phys. (Russ.) vol. 51, 925 (1981)
20. R.AZIZOV, M. KROTOV, V.D. RUSANOV, A.A. FRIDMAN et all., Dokl. Akad. Nauk SSSR, vol. 271, 94 (1983)
21. A.T. BAITEREKOV, V.G. JIVOTOV, M.A. KERIMLUKOV, E.V. MINDUSHEV, D.K. OKTORBAEV, 7th Int. Symp. on Plasma Chemistry, Eindhoven, Netherlands, 1-5.07.1985, p. 742
22. A.JARNOV, V. RODDATIS et all., Khim. Vys. Ener. vol. 20, 510 (1986)
23. A. MIZUNO, A. CHAKRABARTI, K. OKAZAKI, in Non-Thermal Plasma Techniques for Pollution Control, Part B: Electron Beam and Electrical Discharge Processing, NATO ASI SeriesG: Ecological Sciences, vol. 34, Part B, ed. by B.M. Penetrante and S.E. Schultheis, Springer-Verlag, 1993, p. 165
24. A.A. FRIDMAN, A. PETRUSOV, J. CHAPELLE, J.M. CORMIER, A. CZERNICHOWSKI, H. LESUEUR, J. STEVEFELT, J. Phys. III France, vol. 4,1449 (1994)
25. A. CZERNICHOWSKI, Pure and Appl. Chem., vol. 66, 1301 (1994)
26. P. LABBE, F. LAVAL, P. FOUCHER, A. CZERNICHOWSKI, H. LESUEUR, J. Symp. Atlanta, Georgia, Ind. & Eng. Chem. Div. of Am. Chem. Soc., 27-29. 09. 1993, ed. D.W. Tedder, vol. II, p. 399
27. T. CZECH, A. CZERNICHOWSKI, J. MIZERACZYK, Int. Flame Days - Clean Combustion of Waste and Non-Conventional Fuels, Biarritz (France), 16-18.03.1994, paper No. 45, 5 pp.

28. A. CZERNICHOWSKI, T. OPALIŃSKA, B.V. POTAPKIN, ibid., paper No 46, 9 pp.
29. P. CZERNICHOWSKI, A. CZERNICHOWSKI, 8eme Coll. Universite-Industrie "Les techniques electriques et la qualite du sechage", Bordeaux-Talence, France, 16.06.1994, p. B1-1
30. A. CZERNICHOWSKI, A. GORIUS, A.CHARAMEL, B.V. POTAPKIN, The First Int. Conf. on Advanced Oxidation Technologies for Water and Air Remediation, London, Ontario, Canada June 25-30, 1994, p. 247
31. A. CZERNICHOWSKI, T. OPALIŃSKA, P. CZERNICHOWSKI, H. LESUEUR, accepted to the ACS Special Symp. on Emerging Technologies for Hazardous Waste Management VI, Atlanta, Georgia, 19-21.09.1994
32. J. JANCA, B. DOKOUPILOVA, P. MALCIK, A. CZERNICHOWSKI, H. LESUEUR, Czech Application PV 2294-93
33. T. JANOWSKI, A. NAFALSKI, J. WAWSZCZAK, K. BESSHO, Papers of Techn. Meeting on Appl. Magnetics in Japan, vol. MAG-82, 1982, p. 11
34. T. JANOWSKI, H.D. STRYCZEWSKA, Polish Application P-300032
35. T. JANOWSKI, H.D. STRYCZEWSKA, Polish Application P-301836
36. H. LESUEUR, A. CZERNICHOWSKI, Int. J. Hydrogen Energy, vol. 19, 139 (1994)
37. H. LESUEUR, A. CZERNICHOWSKI, M. GRANOPS, 11th Int. Symp. on Plasma Chemistry, Loughborough, England, 22-27.08.1993, p. 752

EFFECTS OF HIGH AC MAGNETIC FIELD STIMULUS TO THE DEVELOPMENT AND BEHAVIOR OF THE NEMATODE

S. YAMADA, T. HASHIGUCHI, R. HOSONO*, and K. BESSHO

Lab. of Magnetic Field Control & Applications, Faculty of Technology,
Kanazawa University, Kodatsuno 2-40-20, Kanazawa 920, Japan
* School of Medicine, Kanazawa University, Takaramachi,Kanazawa 920,Japan

Introduction

By increasing use of electromagnetic devices, many electromagnetic field sources such as MRI machines and superconducting devices, exist in our environment. For example, the influences of the high voltage transmission on the human body have been paid attention. On these circumstances, the influences between the exposure to ac magnetic fields and live organisms have been studied and reported [1]. However, no definite results exist in spite of the possibility of effects against live organism. It is becoming increasingly important to establish standards that explicitly state the safety level for a high ac magnetic field.

The proper choices for apparatus to produce a high ac magnetic field and of desirable organisms enable us to examine the effect of magnetic fields on the human body. At first, we have developed the new apparatus to produce a high ac magnetic field up to 5 T_p (peak value) [2]. Next, the free-living soil nematode, *Caenorhabdities elegans* (*C.elegans*), has suitable qualities for study on the effect of magnetic fields on living organisms. Because it has a small and simple body structure. In addition, the organism is easy to culture in the laboratory and has a short life span. These permit us to test the effects of ac magnetic fields on the live organism [3,4].

We systematically examined the effects of the electromagnetic field on the *C.elegans* life cycle including development, reproductive system, and behavior. This paper explained the experimental device, the approach, and described the results we obtained.

1. Magnetic field generator and nematode

1.1 High ac magnetic field generator

We have developed a high ac magnetic field generator based on the magnetic shielding effect using eddy currents as shown in Fig.1 [2]. When an input voltage with a commercial frequency is applied to the exciting coil, the magnetic shielding by eddy currents is induced into the cylindrical conducting frame and ac magnetic flux is concentrated at an air hole. Figure 1(b) shows the high magnetic field area for testing. Two kinds of water cooling system are installed for cooling conducting frame made of copper and keeping temperature around the experimental area. Then the temperature around the biological testing area is kept to be 20 degrees. Temperature control is necessary since a worm is very sensitive to temperature. Figure 2 shows the characteristics of ac magnetic fields versus an applied voltage. The uniformity of magnetic field in the testing area is over 97 percent and the field has the z-direction. For our biological testing, the magnetic field of 60 Hz was used.

1.2 The nematode as testing worm

The nematode, *C.elegans*, has been used in many biological experiments and is shown in Fig.3. In this study, the wild-type nematode, so-called N2, was used. The majority of nematode are hermaphrodite, the combination of male and female, and the male is produced at the probability from 1/500 to 1/700. The body size is about 1 mm in length and 0.1 mm in width. At about 48 hours after the larva hatches, the worm becomes an adult and starts to lay eggs. The nematode eats colon bacilli on the agar plate and its life length is 2 weeks under 20 degrees centigrade. The nematode moves actively all the time to eat bacilli.

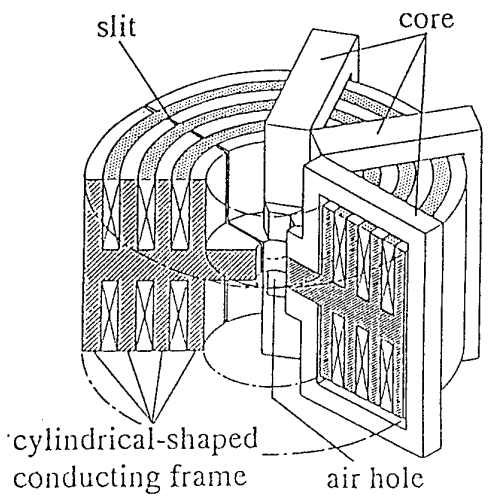

(a) Outline of the generator

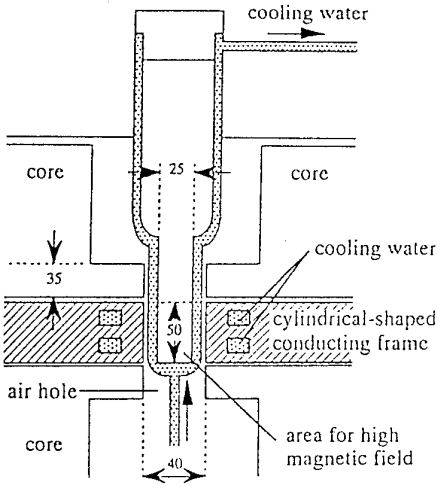

(b) Testing area and cooling system

Figure 1 High ac magnetic field generator.

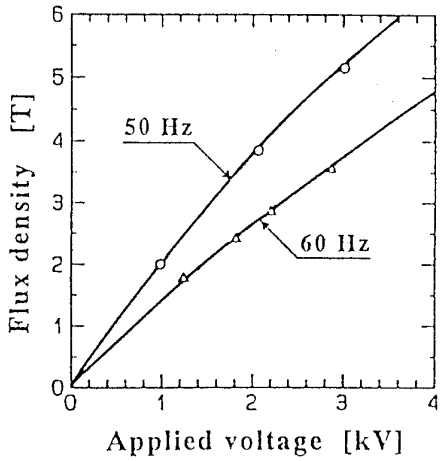

Figure 2 High ac magnetic fields by the new generator.

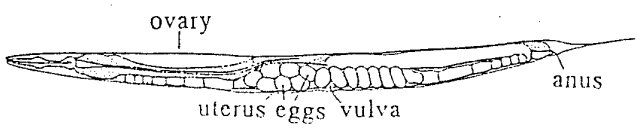

(a) Hermaphrodite

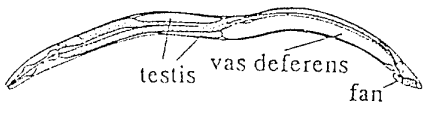

(b) Male

Figure 3 The nematode, *Caenorhabdities elegans*.

Figure 4 shows the life schedule of *C.Elegans*. Cell division occurs at a very rapid rate until 48 hours after the larva stage and the nematode lays egg from 48 to 108 hours. An ac magnetic fields are exposed repeatedly at some intervals until 108 hours. Under these circumstances, the influences of the development and differentiation processes by the exposure to ac magnetic fields have been examined.

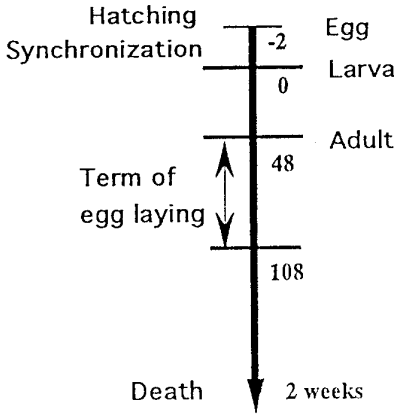

Figure 4 Life cycle of the nematode.

2. Reproduction and development of the nematode

2.1 Influences of reproduction

First the number of progeny is tested for *C.elegans* which is exposed to an ac magnetic field. The worms of the same generation within 2 hours were exposed to ac magnetic fields. The exposures were carried out after the larva stage and continued repeatedly until the egg laying stage. The magnitude of magnetic flux density is 1.7 T and the duration time is 3 minutes. The intervals of the exposure are 6, 8, 12, and 24 hours. Figure 5 shows the influence of the exposure to the number of progeny. The exposed time indicates the total time of the repeated exposures. It is well-known that a nematode produces about 300 eggs. The worm without exposure to an ac magnetic field , so-called *control* group, has the same number of progeny. As shown in Fig.5, the number of progeny was decreased in proportion to the exposed time. For 27-min *exposed* group, the 10.3 percent decrease was obtained.

Next the influence of magnetic field stimulus to egg laying schedule was tested. The nematode grows as adult at about 48 hours after the hatching stage and starts to lay egg. We select 20 worms with the 170-min exposure to 1.2 T magnetic field and the *control* group without exposure. At each interval of 12 hours, we count the total number of egg until egg

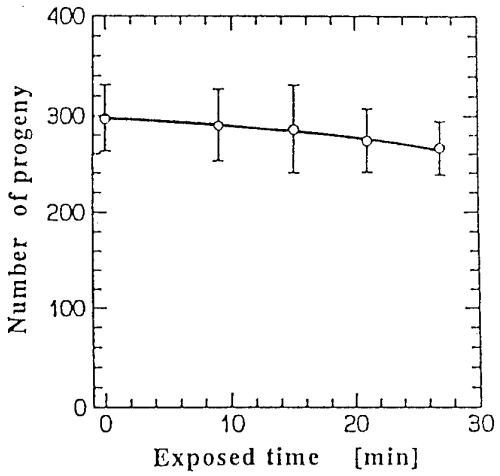

Figure 5 Number of progeny versus the exposed time of magnetic field.

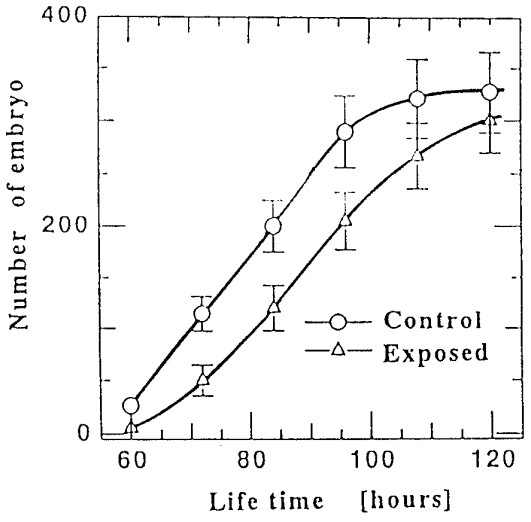

Figure 6 Number of embryo versus life time by the exposure to an magnetic field.

laying stops. Figure 6 shows the egg laying process between two groups. The number of embryo denotes the average values of 20 worms. The result shows that the start of egg laying is delayed by the exposure and the difference of the total egg is 9 percent.

2.2 Influences of development

To examine the influence of the magnetic field to development, we have investigated the body size of the nematode. The tested worms were exposed to the 1.2 T magnetic field with the 10-min duration. The exposures were done 9 times at the intervals of 6 hours. We chose each 10 worms for the *exposed* and *control* groups. Figure 7 shows the influence of body length after the exposure. The delay and decrease of growth are observed clearly. The result in Fig.7 definitely relates to the influence of reproduction.

3. Behavioral effects by the exposure to an ac magnetic field

3.1 Influence of behavioral responses

The behavioral responses of worms exposed to an ac magnetic field were observed. The nematode moves actively to get food between 72 and 100 hours after the larva stage. During this period, the worm is exposed to the ac magnetic field and its behavior is observed according to the time schedule shown in Fig.8. Before the exposure, we check the normal movement of the worms. The worm simply moves at random with a sinusoidal trajectory. After the exposure to a magnetic field of 1.2 T and a frequency of 60 Hz, the movement of the worms was recorded at the interval of 3 minutes. 41 worms were observed and were classified into 3 types. For comparison, we observed the behaviors of the 21 worms using the same procedure described above but without exposure to an ac magnetic field. Figure 9 shows the behavioral patterns at the interval of 3 minutes before and after exposure to the magnetic field. These figures show the following three typical behavioral patterns,

Type 1 ; There is no change before and after exposure to the magnetic field.
Type 2 ; There is an active behavior with abnormal forward-backward motion after the exposure.
Type 3 ; Sluggish motions can be observed

Figure 10 shows the ratio of three types of behaviors. The 49 percent of worms have the type 2 and type 3 behaviors. Compared to the *control* group without the exposure to an ac magnetic field, the motional activities of the exposed worms are significantly affected. Then the worm were rested for 10 minutes after which their behaviors were observed again. Two of the observed 10 worms recovered and the others continued to exhibit the same behavior.

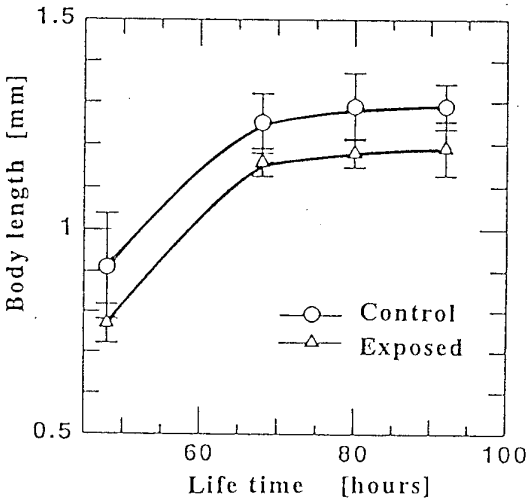

Figure 7 Influence of body length.

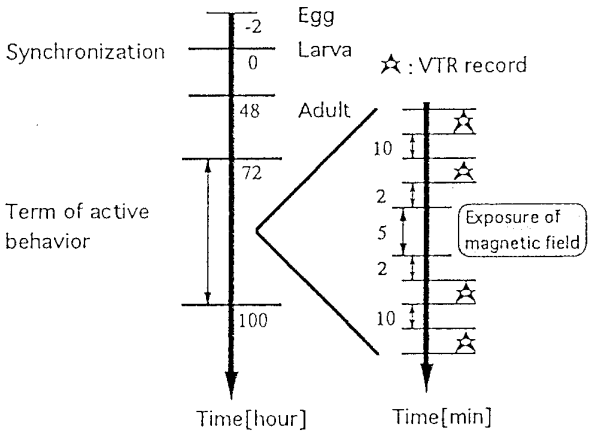

Figure 8 Time schedule 1 for test.

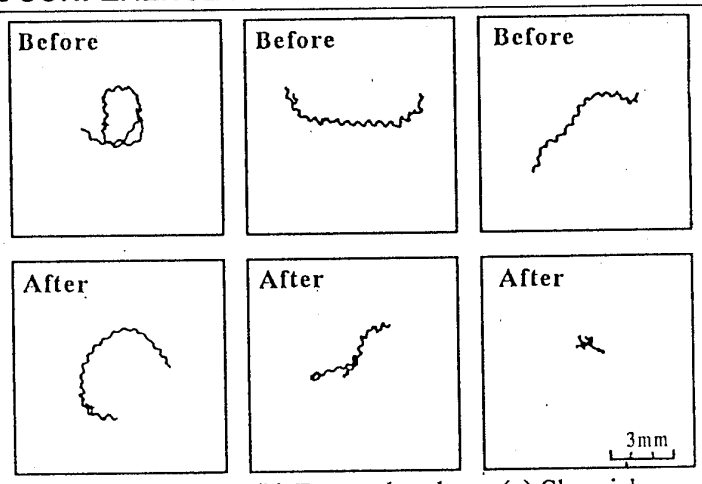

(a) No change. (Type 1) (b) Forward and backward motion(Type 2) (c) Sluggish motion (Type 3).

Figure 9 Three types of trajectories at the interval of 3 minutes in response to the exposure to ac magnetic field.

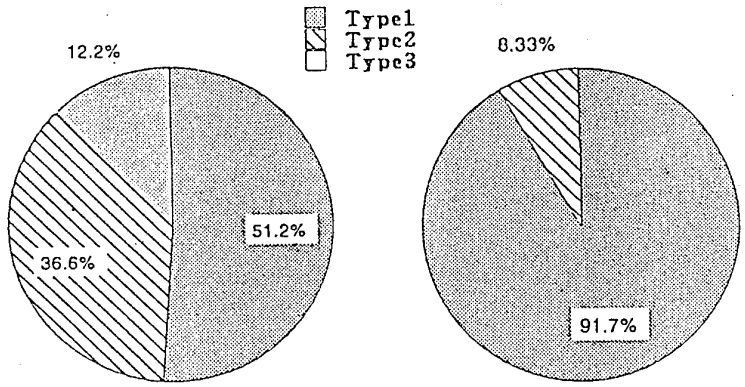

Figure 10 Ratio of motional patterns. The *control* and *exposed* groups have the same environment except for the exposure to magnetic field.

3.2 Effect on eating behavior

In order to specify the behavior of the worm, we attract the movement by providing it with colon bacillus as food. We prepare the agar culture medium in which colon bacilli are gathered at the center as shown in Fig.11. We divide the nematodes into two groups, the *control* group and the *exposed* group. The two groups have the same culture conditions but the *exposed* group are exposed to a magnetic field. After the animals are exposed to a magnetic flux density of 1.2 T and at a frequency of 60 Hz and for a period of 5 minutes, we observed the movement of the animal from point *A* to the food area. The testing schedule is shown in Fig.12. Before exposure, the worm was prevented from getting food for a period of 4 hours.

Figure 13 shows the trajectories of locomotive behavior. We observed two typical types of behaviors. The normal animals have a movement from *A* to the food area as shown in Fig.13(a). The other animals have a sluggish movement but exhibit a repetitive backward-forward locomotion as shown in Fig.13(b). This shows that the behavioral activity of the exposed animals is significantly affected. Figure 14 shows the ratio of animals that arrive at the food area. The differences between the *control* and *exposed* groups for an initial period of 3 minutes are not observed. The 90 percent of the *control* animals which were exposed to magnetic field arrived at the food area. But for the *exposed* group, only 55 percent of the animals arrived at the food area.

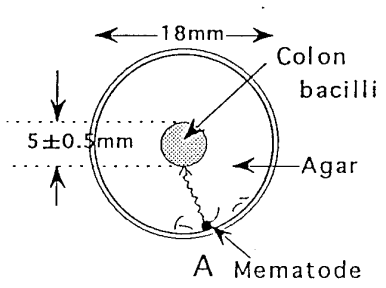

Figure 11 Agar plate for test.

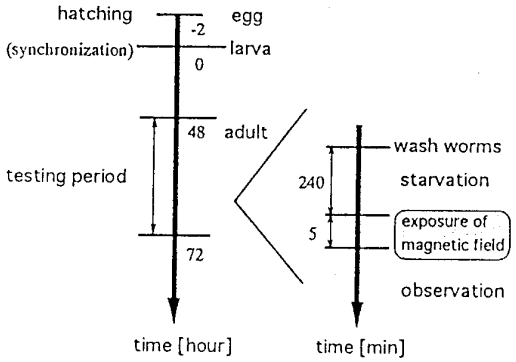

Figure 12 Time schedule 2.

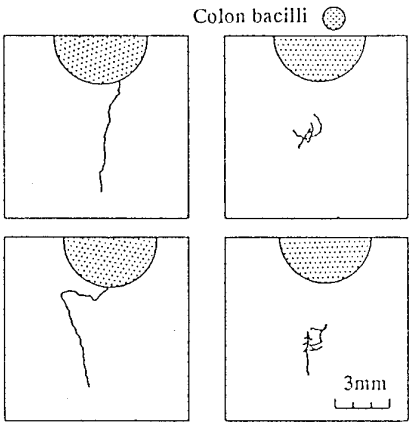

Figure 13 Behavioral trajectories.

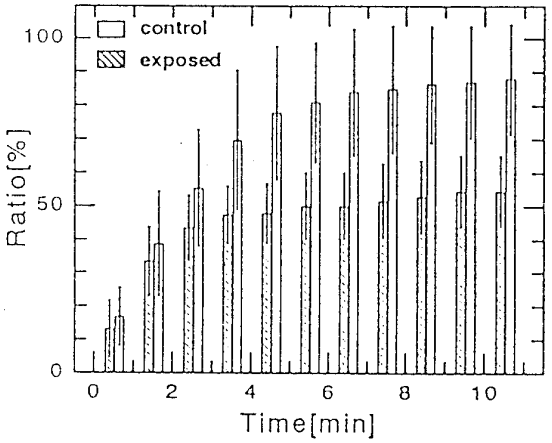

Figure 14 Ratio of animals that arrived at the food area.

4. Conclusions

This paper described the effect of an ac magnetic field to the reproduction, the development, and the behavioral response of the nematode. We have clearly observed the apparent differences between the *control* and *exposed* groups of warms at each results. The value of the magnetic field in the experiments is extremely larger than one in the normal circumstances. It is clear that the influence of the exposure to an ac magnetic field was enhanced in our testing. According to our estimation, these changes are not caused by a default in the muscle system but probably by a fault in the sensory system. Further studies are required to evaluate the mechanism by which the magnetic field effects the organisms.

References

1. K.Fizgerald, I.Nair, G.Morgan, Electromagnetic fields ; the jury's still out, IEEE Spectrum, August, (1990).
2. K.Bessho, S.Yamada, M.Kooto, "Characteristics of a Multilayer Eddy-Current-Type Ac Magnetic Coil with a Cooling System", J. Appl. Phys., 64, 10, 6020-6022, '88.
3. T.Kunitani, and etal., Development and differentiation of the nematode C.elegans in ac high magnetic field, JIEE Magnetics Meeting, MAG-92-107, (1992), in Japanese.
4. K.Bessho, S.Yamada, "Development and behavior of the nematode in the ac magnetic field", JIEE Magnetics Meeting, MAG-93-80, (1993), in Japanese.

DETERMINING THE RESPONSE OF POWER TRANSMISSION AND DISTRIBUTION LINES TO A NUCLEAR DETONATION AT A HIGH ALTITUDE

Zdzislaw W. Trzaska
Department of Electrical Engineering, Warsaw University of Technology,
00-601 Warsaw,Poland,Fax:()(48)(2)6284568, Phone:()(48)(2)6284568
E-mail:trzd@plwatu21.bitnet

September 6, 1994

ABSTRACT

A nuclear detonation at a high altitude above the earth's surface would produce an intense transient electromagnetic field and developing a high altitude electromagnetic pulse environment. The levels of transient electrical surges in power system distribution lines play an important role in determining the overal response of the electrical power network to a high (above 100 km) altitude electromagnetic pulse.

This paper deals with a method for determining the response of a multiconductor transmission and/or distribution line to a high altitude electromagnetic pulse excitation.

The established calculational model may be used to perform all needed studies to determine possible responses of the power system to a nuclear detonation at a high altitude.

1 INTRODUCTION

A transformation has been taking place during the past few years in the market of radioactive materials. This fact introduces a great probability of hazards of a high altitude nuclear explosion. Such an effect would result in the excitation in the earth environment of an intense electromagnetic pulse which propagated to the earth's surface may cause severe damages of various elements constituting power systems.

As power systems increased in size, so did the number of lines, substations, transformers, switchgears, and so on. Their operation and interactions became more complex. Usually neighboring power companies are interconnected by one or more transmission lines called tie lines as depicted graphically in Fig.1. Interconnections are made so that operating areas can share generation and load.

The interactions between the intense electromagnetic pulse generated by a high

altitude nuclear explosion and the power system include those at the transmission and distribution lines as well as in such system components as transformers, switchgears, and in the internal electronics. Important effects at the transmission lines and in transformers include degradation of dielectric materials which can result in transient producing arc-discharges. For these external effects the characterization of the free-excitated environments as a function of a space-distribution of the electromagnetic pulse and time are important.

The internal effects of a high altitude nuclear explosion in power systems are performance degradations resulting from energy disposition by accumulated ionization in the semiconductor materials. Therefore, of particular interests for effects on the power systems of high altitude nuclear explosions are the propagation of induced voltages along the transmission and/or distribution lines. For this purpose, the appropriate model of a high altitude electromagnetic pulse coupling to overhead lines has beeen established and studied. The involved model yields responses which can be used to illustrate features of the high altitude electromagnetic pulse coupling processes and overall line behavior. A multi-velocity analysis was performed and the results are compared with those arising from a single velocity analysis, with the velocity being that of the common mode. A difference between the two results was noted.

2 PROBLEM STATEMENT

Exposure of devices and circuits to an intense electromagnetic pulse induced in space causes the insulating and semiconducting materials to be ioniozed which leads to transient and permanent changes in device electrical properties.

On power transmission lines which are designed with a higher basic insulation level, the possibility of line flashover is smaller, but it must be recognized that these lines may run for many kilometers and, consequently, can deliver a large amount of electromagnetic pulse energy into a substation or other facility.

Analysis of power systems is based on mathematical representations for the electric components used to generate power, distrbute it, and consume the power. In general, linear representations are used to study the behavior of the circuits due to small disturbance, then when appropriate, nonlinear models are employed to investigate response due to large disturbance.

Three-phase transmission lines (Fig.2) are used to transfer power from a point of generation to a point of consumption. The voltages levels or potentials are usually selected to be as possible to minimize transmission losses.

In both transmission and distribution lines, the relatively uniform line geometry is interrupted periodically by towers, which can present a conducting path from the neutral or shield wires to ground. The complexity of these lines suggests that a simple, two-wires transmission lines model is not adequate, and that a multiconductors model is needed to accurately predict the electromagnetic pulse surges on transmission and distribution lines. This model and its use are described in this paper.

In a general case of a multiconductor transmission or distribution line its model contains n parallel long conducting wires located over a perfectly conducting earth (Fig.3a).

The towers and/or transformers are modelled by a set of impedance elements between each conductor and the earth, as is shown in Fig.3b. There are $p+1$ towers positioned at $x = 0, L, 2L, ..., pL$. After the $(p+1)-th$ tower a line is considered as semi-infinite. Each segment of the line between two neighboring towers is represented by a uniform ladder network composed of $m \geq 1$ multiports characterized by a series impedance matrix $\mathbf{Z}(s)$ and transversal admittance matrix $\mathbf{Y}(s)$ as is shown in Fig.3c, respectively.

Generalizing the method presented in [1] to the multivariable case we can describe the multiport ladder network between two neighboring towers by the following matrix equation

$$\begin{bmatrix} \mathbf{V}(k+1) \\ \mathbf{I}(k+1 \end{bmatrix} = \mathbf{A}^k \begin{bmatrix} \mathbf{V}(k) \\ \mathbf{I}(k) \end{bmatrix} \tag{1}$$

where $k = 0, 1, ..., p$ and $m \geq 1$ denotes the number of multiports in the ladder network.

Matrix $\mathbf{A} = \mathbf{A}(s)$ depends on the line parameters as follows

$$\mathbf{A} = \begin{bmatrix} 1 + \mathbf{Z}(s)\mathbf{Y}(s) & \mathbf{Z}(s) \\ \mathbf{Y}(s) & 1 \end{bmatrix}$$

Denoting

$$\mathbf{Q} = \mathbf{Z(s)Y(s)} \tag{3}$$

and applying the procedure presented in [2] we can easy express the $k-th$ power of the chain matrix $\mathbf{A}(s)$ and obtain

$$\mathbf{A}^k(s) = \begin{bmatrix} T_k(\mathbf{Q}) & \mathbf{Z}P_k(\mathbf{Q}) \\ \mathbf{Y}P_k(\mathbf{Q}) & T_{k-1}(\mathbf{Q}) \end{bmatrix} \tag{4}$$

where $T_r(\mathbf{Q})$ and $P_s(\mathbf{Q})$, $r, s = 0, 1, 2, ..., m$ denote polynomials in $\mathbf{Q}$ of the degrees r and s, respectively.

They are determined by the following recurrence relations

$$T_r(\mathbf{Q}) = (2 \cdot \mathbf{1} + \mathbf{Q})T_{r-1}(\mathbf{Q}) - T_{r-2}(\mathbf{Q}),\ r = 2, 3, ..., \tag{5}$$

with $T_0(\mathbf{Q}) = \mathbf{1}$ and $T_1(\mathbf{Q}) = \mathbf{1} + \mathbf{Q}$

and

$$P_s(\mathbf{Q}) = (2 \cdot \mathbf{1} + \mathbf{Q})P_{s-1}(\mathbf{Q}) - P_{s-2}(\mathbf{Q}),\ s = 2, 3, ..., \tag{6}$$

with $P_0(\mathbf{Q}) = \mathbf{0}$ and $P_1(\mathbf{Q}) = \mathbf{1}$.

For example, if we fixe $r = s = 4$ then we have

$$T_4(\mathbf{Q}) = \mathbf{1} + 10\mathbf{Q} + 15\mathbf{Q}^2 + 7\mathbf{Q}^3 + \mathbf{Q}^4$$
$$P_4(\mathbf{Q}) = 4 \cdot \mathbf{1} + 10\mathbf{Q} + 6\mathbf{Q}^2 + \mathbf{Q}^3$$

It is easily seen that matrix polynomials $T_r(\mathbf{Q})$ and $P_s(\mathbf{Q})$ fulfill the relation

$$T_h(\mathbf{Q})T_{h-1}(\mathbf{Q}) - \mathbf{Q}P_h^2(\mathbf{Q}) = \mathbf{1}, h = 1, 2, ... \tag{7}$$

Some other interesting and important relations for polynomials $T_r(\mathbf{Q})$ and $\mathrm{P}_s(\mathbf{Q})$ can be established but for the the sake of presentation simplicity they are omitted here. For details see for example [3].

Assembling appropriate multiport networks yields the complete model of the studied system. It is shown in Fig.3c, where $\mathbf{Z}_t$ characterizes the multiport element which corresponds to the tower and $\mathbf{Z}_s$ represents the semi-infinite part of the line.

It is worth noting that the established model is suitable for computer simulations because it takes integral space-discrete nature.

Following the above established model we can express the vectors of the conductor potentials $\mathbf{V}(r)$ and currents $\mathbf{I}(r)$ along the system by the following recurrent equations

$$\begin{bmatrix} \mathrm{V}r+1) \\ \mathrm{I}(r+1) \end{bmatrix} = \begin{bmatrix} \mathbf{A}_1 & \mathbf{B}_1 \\ \mathbf{C}_1 & \mathbf{D}_1 \end{bmatrix} \begin{bmatrix} \mathbf{V}(r) \\ \mathbf{I}(r) \end{bmatrix} \tag{8}$$

where

$\mathbf{A}_1 = \mathbf{A}_1(\mathbf{Q}) = T_k(\mathbf{Q}) + \mathbf{Z}P_k(\mathbf{Q})$, $\mathbf{B}_1 + \mathbf{B}_1(\mathbf{Q}) = \mathbf{Z}P_k(\mathbf{Q})$, $\mathbf{C}_1 = \mathbf{C}_1(\mathbf{Q}) = \mathbf{Y}P_k(\mathbf{Q}) + T_{k-1}(\mathbf{Q})\mathbf{Y}_t$, $\mathbf{D}_1 = \mathbf{D}_1(\mathbf{Q}) = T_{k-1}(\mathbf{Q})$

represent matrices of one segment in the model.

Using the above equations successively for $r = 1, 2, ..., p+1$ we determine the distributions both voltages and currents along the system. An another way of using the above equations for a given node lies in evaluating respective powers of the coefficient matrix of equations (8).

3 INCIDENT FIELDS OF HIGH ALTITUDE ELECTROMAGNETIC PULSE

The high altitude electromagnetic pulse is a complicated function of time and position under the explosion location [4]. Such a pulse induces an incident electromagnetic field which can be divided into two parts: a horizontally polarized and vertically polarized parts. The relative amounts of each component depend on both the explosion and observation locations, as well as the location of the earth's mgnetic field in the neighboring of the source region.

A typical time domain waveform of the incident electric field component is shown in Fig.4. This waveform is incident on the transmission line with angles of incidence α and β, as shown in Fig.5. Now it is evident that the form of the assumed, in our studies, field is planar and it acts on the line conductors and the loads. Moreover, we must add to the incident field a field reflected from the earth. Decomposing the incident field into its Fourier spectral components it is possible to compute for each frequency ω the earth-reflected field component. Thus all calculations can be performed in the complex frequency domain and by using an inverse Fourier transform we determine the final transient response of the transmission or distribution line to the total excitation.

The x-directed field just on the surface of the earth can be represented by the expression

$$E_x(x, y, z) = E_x(y, z)e^{-\gamma x \cos\alpha \cos\beta} \tag{9}$$

where $E_x(y, z)$ denotes the field magnitude in the plane $x = 0$ and $\gamma = j\frac{\omega}{c}$ is the free-space propagation constant with c as the speed of the light. In a similar manner we can represent the vertical (y-directed) total electric field component on the surface of the earth

at a point (x, y, z) and obtain

$$E_y(x, y, z) = E_y e^{-\gamma x \cos\alpha \cos\beta} \tag{10}$$

for the vertically polarized incident field. This vertically polarized component excitates the vertical conductors of the loads on the ends of the multiconductor lines.

4 RESULTS

The slution for a field-excited multiconductor line can be obtained by first considering the response of the line at a lumped n-vector voltage source located at an arbitrary position x_0 on the line. Next we can aplly this solution as a discrete-continuous Green's function and compute the response over all segments of the line with the excitation provided by the incident high altitude electromagnetic pulse.

The incident field is assumed to arrive at the earth at $x = 0$ at a time $t = 0$. This implies that the zero-initial conditions along the line and at $t = 0$ the line starts to rise in accordance with the behavior of the incident field. In using the model presented in the previous sections it is important to shift the starting time of the response to an appropriate delay which is determined by the coefficient $e^{-x_k \gamma \cos\alpha \cos\beta}$ with x_k being the position of the end of the $k - th$ section of the line.

Detailed calculations have been performed fo a 3-phase line $400kV$ transmission line. This line is assumed to be illuminated by the electromagnetic pulse of Figs.4 and 5 with $\alpha = \frac{\pi}{4}$ and $\beta = 0$. For this case a semi-infinite line was considered with the open-circuit voltage on the three-phase conductors and on the ungrounded shield conductors being computed. The resulting transient responses are shown in Fig.6. A negligible difference between results of calculations for a multi-velocity and a single-velocity analysis was noted.

5 CONCLUSIONS

In this paper we have presented a more realistic model with respect to up-to-date known ones for a transmission or distribution line interacting with an intense electromagnetic pulse induced by a high altitude nuclear explosion. The model offers possibilities of including such important components of the power systems as transformers, towers, shield wires, substations equipments, and other ones. This calculational model has been used to perform a detailed study of possible line response without involving nonlinearities. Detailed calculations of line responses for all possible line locations and orientations in the illuminated region on the earth's surface are under further investigations.

References

[1] Z. Trzaska: On numerical triangles showing links with Chebyshev polynomials. Proc. C. Lanczos Cent. Int. Conference, Raleigh, 12-17 Dec. 1993

[2] Z. Trzaska: Modified numerical triangles and their applications in analysis of dynamical systems.(in Polish). Proc. XVI SPETO, Gliwice-Wisla,May 15-18, 1993

[3] Z. Trzaska: On the Fibonacci hyperbolic trigonometry and modified numerical triangles. The Fibonacci Quarterly (in print) A criterium for optimal matching of a three-phase load to a supplying system. Electrotechnical Review (in Polish). 1990, Nr 10,pp.225-228

[4] W.J. Karzas and R. Latter: Electromagnetic Radiation from a Nuclear Explosion in Space. Phys. Rev., vol.126, 1962, Nr 6, pp. 919-926

[5] K.W. Klein, P.R. Barnes, and H.W. Zaininger: Electromagnetic Pulse and the Electric Power Network. IEEE Trans. Power Appar. Syst., vol. PAS-104, 1985, Nr 6, pp. 2286-2274

[6] T.V. Zahle: A simple way to determine the driving point impedance function of an n-port. IEEE Trans. Ac. Sp., vol. AS-21, 1974, Nr 3, pp.456-458

[7] J. R. Srour, and J.M. McGarrity: Radiation Effects on Microelectronics in Space. Proc. IEEE, vol.76, 1988, Nr 11, pp. 1443-1469

[8] G.L. Kusic: Computer-aided Power Systems Analysis. Prentice-Hall, Englewood Clifs, N.Jersy, 1986

[9] Z. Trzaska:A criterium for optimal matching of a three-phase load to a supplying system. Electrotechnical Review (in Polish). 1990, Nr 10,pp.225-228

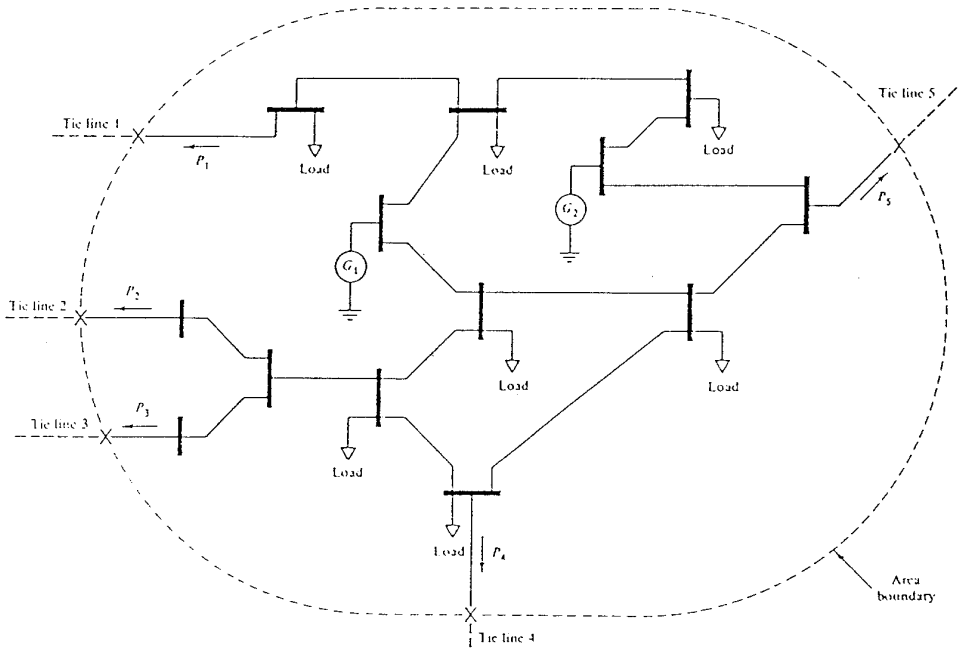

Fig.1. An interconnected power system

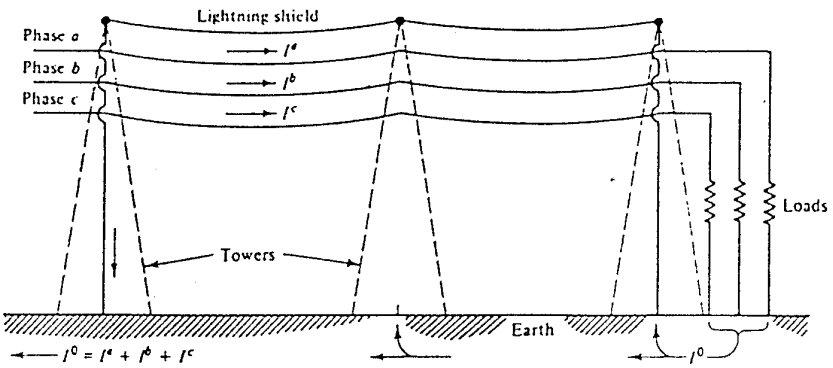

Fig.2. A thre-phase transmission line

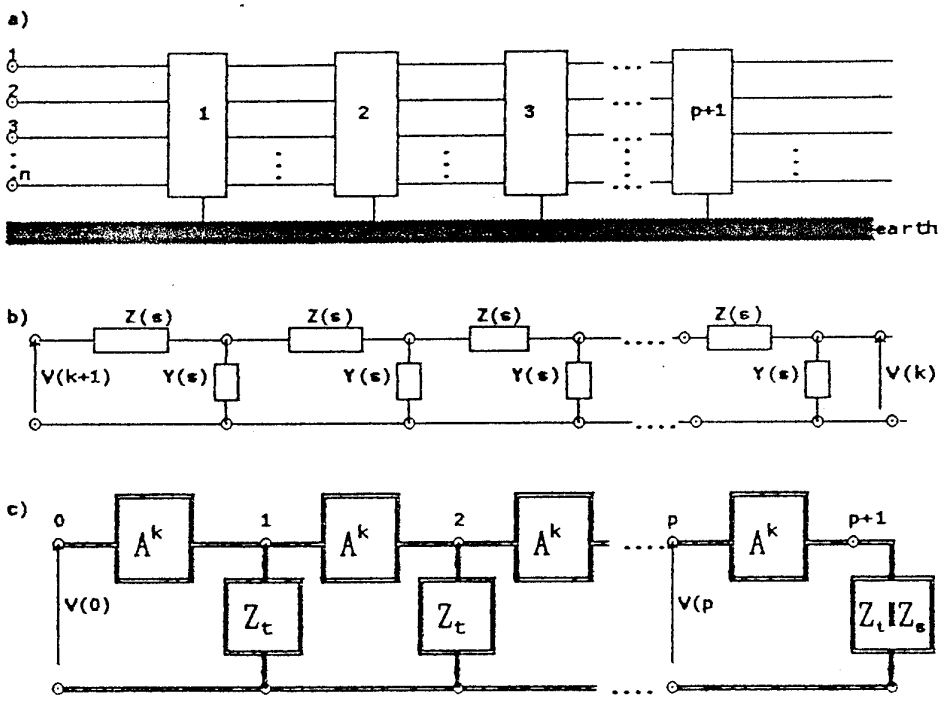

Fig.3. Model of a multiconductor transmission or distribution line with periodically distributed loads

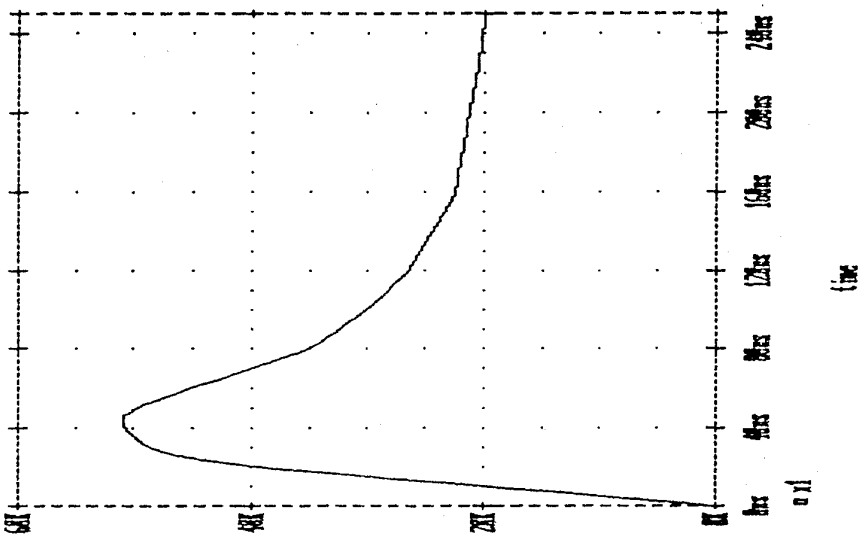

Fig.4. Time-evolution of a high altitude electromagnetic pulse

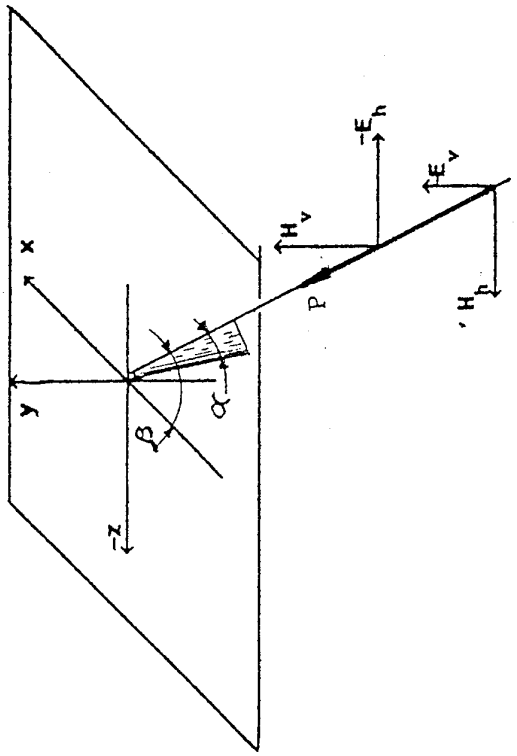

Fig.5. Space orientation of a plane electromagnetic wave

Fig.6. Results of calculations of a response of a semi-infinite line

Ryszard Goleman
Maciej Pańczyk
Mirosław Pawłot
Lublin Technical University

SIMULATION OF MAGNETIC FIELD DISTRIBUTION IN A MODEL OF A HYBRID HIGH-SPEED INDUCTION MOTOR

1. Introduction

Rotational speed range of electrical machines is very wide from a fraction of revolution per minute to hundreds of thousands of revolutions per minute. Electrical motors can be grouped according to their rotational speed. The following groups can be distinguished:

— low-low-speed motors - their rotational speed does not exceed 1 rev/s,
— low-speed motors - 1-5 rev/s,
— high-speed motors - 5-50 rev/s,
— high-high-speed motors with rotational speed exceeding 50 rev/s.

Recently, a few works presenting models of high-speed motors that combine features of magnetic multipliers and classical engines have been published. Up till now models of shaded-pole induction motors [1,11], permanent-split capacitor motors [3,4,5] and motors with three-phase power supply [7,10,11] have been developed. These new solutions are closely connected with research on magnetic frequency multipliers and especially on triplers based on three-column cores. In frequency multipliers voltage of elevated frequency is obtained from terminals of adequately connected windings whereas in a hybrid motor higher harmonic flux, which is a working flux, has to be directed to the rotor region. It makes the construction of the stator circuit difficult. When designing high-speed hybrid motor models one should know the value of magnetic induction of individual elements of magnetic core. Direct adaptation of already known dependences to determine magnetic field distribution is impossible because of complicated structure of magnetic circuit and its non-linearity. The presented work aims at numerical calculation of magnetic induction distribution in magnetic core of a high-speed induction motor which applies the third harmonic of magnetic flux for various values of current density in windings.

2. Models of hybrid high-speed motors

High-speed synchronous motor supplied from a 50 Hz network is a combination of frequency multiplier and one-phase AC motor and that is why it is called high-speed hybrid induction motor.

Magnetic circuit of the stator is composed of a 3-column core of a single-phase frequency tripler. The rotor of this induction motor is placed in the middle column of magnetic core that forms salient poles and this way tripler and motor have a common magnetic circuit which simplifies the structure (Fig. 1).

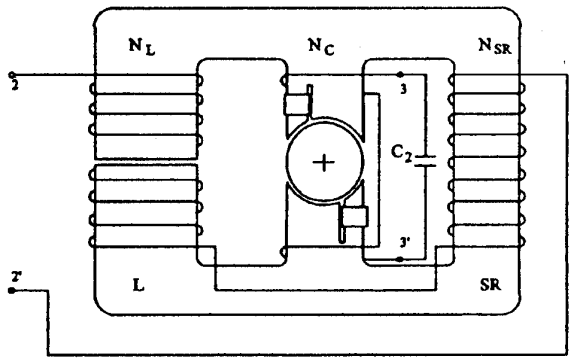

Fig.1. High-speed hybrid induction motor [11].

Two columns have primary windings N_L and N_{SR} connected in series. A column with air gap (L) and winding N_L functions as a linear choking coil whereas a column denoted SR with N_{SR} winding and cross-section smaller than the one of the L column serves as a non-linear choke.

A motor with single-phase supply has two disadvantages: small starting torque and small efficiency. Hybrid motor with , revolving field approximating a circular one was proposed as a solution to avoid the mentioned disadvantages. In the motor's magnetic circuit a two-phase frequency tripler was applied to generate the third harmonic of magnetic flux. In the tripler Scott-connection was applied to connect primary windings of two triplers from the Fig. and this way a 90° phase shift of the basic harmonic (60 Hz) fluxes in the cores of both triplers was obtained. Third harmonics of the fluxes have phases that differ by 270° practically independently of the motor's load and rotational speed.

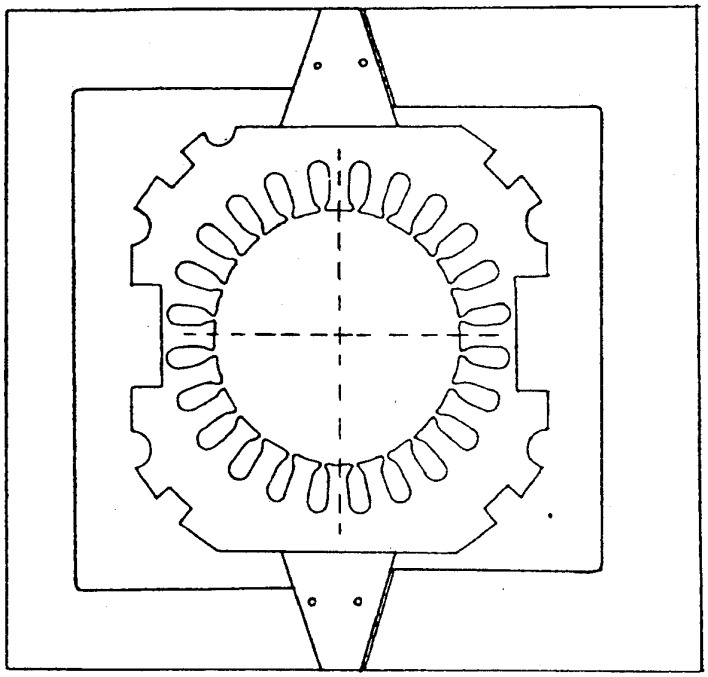

Fig. 2. Structure of a stator in a single-phase hybrid motor.

Salient-pole motors are characterized by non-sinusoidal distribution of magnetic field in the motor's gap. Harmonic fields of the rotor and the stator cooperate and generate torques. Asynchronous torques of higher harmonics are disadvantageous because they reduce the resultant torque and around $s = 1$ they considerably deform the torque's characteristics (local extremes of the torque occur). Synchronous torques (in the diagram, in the function of speed they appear as pulses) can reach high values and can make starting of the motor impossible. The torques at $s < 1$ are less dangerous considering inertia of the rotor that cannot just immediately "get stuck" but passes through critical speed values and reaches subsynchronous speed. Alternating torques can also occur. They disturb steady running of a motor by its acceleration or lagging. For to obtain distribution of the field on the rotor's

surface that is more advantageous than in the mentioned above solutions the Authors propose to apply a slotted stator (Fig.2). Magnetic circuit of such a stator has two columns (linear one and non-linear one) that are magnetized by one current like in the solution of Japanese authors [1,10,11]. Magnetic fluxes in the columns are distorted and contain considerable third harmonic. Fluxes of network frequency (50 Hz) in both columns are in phase and third harmonic fluxes - in counterphase. Difference of the fluxes of both columns is directed to the slotted part of a stator and subsequently to the rotor region. Main and starting windings are located in stator's slots. There is a capacitor connected to the main winding to increase the value of the third harmonic.

3. Numerical calculations

Magnetic field distributions in a motor were determined by means of the finite elements method (FEM) and with the application of the FAT program [12,13]. In view of limitations following from the structure of the program it was necessary to present two quarters of the motor's cross section.

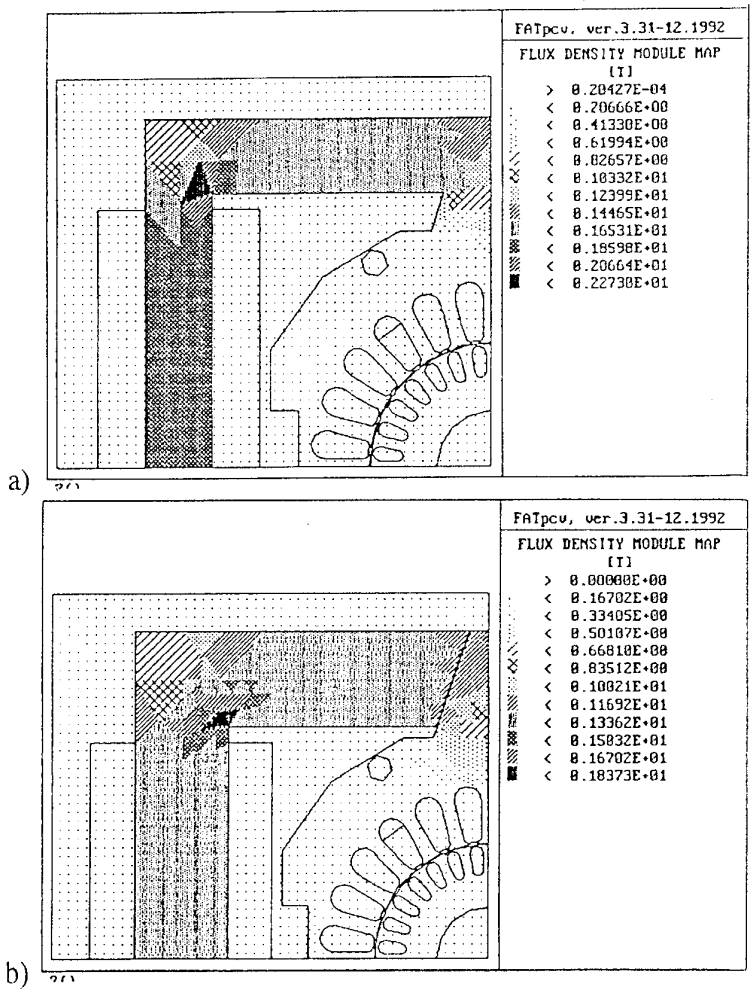

Fig.3. Distribution of magnetic induction modulus in the part of a motor with (a) non-linear choking coil and (b) linear choking coil.

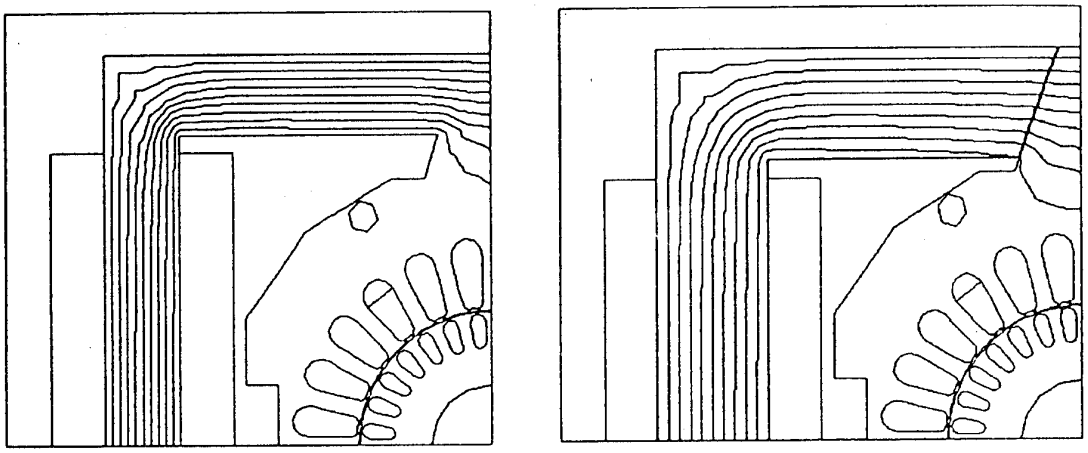

a) b)

Fig.4. Equipotential lines in the magnetic circuit of the part of a motor with (a) non-linear choke and (b) linear choke (current density in choke windings -1.18 A/mm^2).

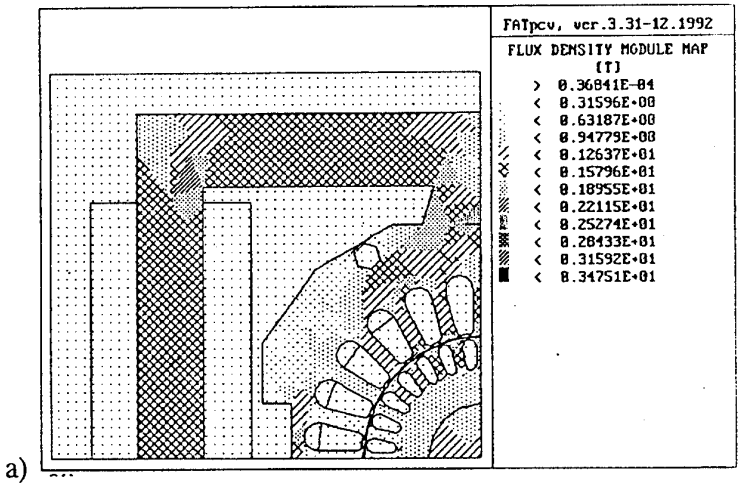

a)

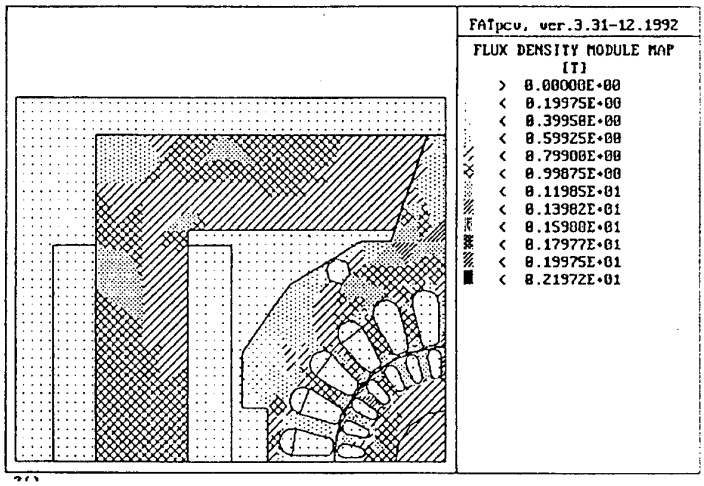

b)

Fig.5. Distribution of magnetic induction in the part of a motor with (a) non-linear choke and (b) linear choke with power supply to choke windings and to the windings in stator's slots.

One of the quarters contained a part of a linear choking coil L and the other one - of a non-linear choke SP. The mesh that contained a linear choke was divided (together with the surrounding area) into 1472 elements and included 773 nodes. The quarter with a non-linear choking coil was divided into 1429 elements and included 752 nodes. Maximum approximation error with such divisions is in the first case - 3.41% and in the other one - 3.38%.

Two kinds of power supply to motor windings were considered. The first one concerned power supply to the windings of chokes and corresponded (approximately) to the distribution of the first harmonic of magnetic flux. The other case combined power supply to choke windings with powering windings in the stator's slots which simulated a real motor operation.

Chosen distributions of magnetic induction and equipotential lines corresponding to the current density in choke windings of 1.18 A/mm^2 are presented in Figs.3,4,5.

4. Conclusions

Simulations of magnetic field distribution in magnetic core of the motor's model indicate that, at given values of current in windings, induction in individual elements of the motor reaches satisfactory values which can ensure its proper operation.

When windings of the columns are powered with a current of 1.18 A/mm^2 density that simulates distribution of the first harmonic of a flux it can be observed that only a small portion of the flux (from 0.011 to 0.045 Wb/m of the rotor's length) gets into the slotted part of the stator. The total first harmonic flux getting into the core that connects magnetic core of the motor's linear and non-linear parts is from 0.018 to 0.036 Wb/m. A flux in the gap between the rotor and the stator that corresponds to the given values is of the order of 0.00017 Wb/1m of the rotor's length.

Magnetic induction in both columns (linear and non-linear one) reaches the highest values in the corners of the internal edges in the columns. Modulus value of magnetic induction is influenced the most by the tangent component of the 1.7 ÷ 1.9 T order (in the non-linear column) and 1.1÷1.4 T (in the linear column).

Maximum values of induction on the stator's and rotor's teeth are below 1.6 T i.e. that the teeth operate in the linear part of the saturation curve.

Normal component of induction in the gap between the stator and the rotor reaches maximum value of 0.7 T and it is dominating.

References

[1] K. Bessho, S. Yamada, T. Sudani, T. Takeuchi, *A new high-speed hybrid AC motor*, Electromechanics and Industrial Electronics Applied Manufacturing Processes Conf.,17-18 Sept., 1985, Latinal, Italy.

[2] M. Dąbrowski, *Fields and circuits of electrical machines* [in Polish], WNT, Warszawa 1971.

[3] R. Goleman, T. Janowski, K. Nalewaj, *Operation and construction elements of high speed induction motors supplied with 50Hz network* [in Polish], 16-th Seminar on Fundamentals of electrotechnics and circuit theory, Vol II, Gliwice -Ustroń, pp. 385-392, 19-22. 05. 1993.

[4] R. Goleman, T. Janowski, M. Pańczyk, *Magnetic field of a high-speed hybrid induction motor model* [in Polish], 17-th Seminar on Fundamentals of electrotechnics and circuit theory, Vol II, Gliwice -Ustroń, pp. 173-178, 25-28. 05. 1994.

[5] R. Goleman, *A high-speed induction motor making use of the third harmonic of the magnetic flux*, Journal of Magnetism and Magnetic Materials, Vol. 133, pp. 624-626, 1994.

[6] T. Janowski, R. Goleman, J. Guz, A. Wac-Włodarczyk, *Open circuit induction of magnetic frequency multipliers*, Scientific Papers of the Electrical Engineering Department LTU, Ser.B, Nr 5, pp. 19-34, 1983.

[7] J. Lu, S. Yamada, K. Bessho, *Harmonic balance finite element method taking account of external circuits and motion*, IEEE Trans. Magnetics, Vol. MAG-27, No.5, pp. 4024-4027, 1991.

[8] M. Pawłot, *High speed asynchronous induction motor supplied from a 50 Hz network* [in Polish], MSc. thesis, Department of Fundamentals Electrical Engineering, Lublin Technical University,1994.

[9] J. Skwarna, *Design problems on case induction motors of high rotational speed* [in Polish], Scientific Papers of the Electrical Engineering Department LTU, Ser.A, Nr 4, 1983.

[10] S. Yamada, A. Takeuchi, K. Bessho, *New high-speed induction motor driven by a commercial source*, IEEE Trans. Magnetics, Vol. MAG-23, No.5, pp. 3020-3022, 1987.

[11] S. Yamada, A. Takeuchi, T. Sudani, K. Bessho, *High-speed AC motor including the function of a magnetic frequency tripler*, IEEE Trans. Magnetics, Vol. MAG-22, No.5, pp. 967-969, 1986.

[12] Field Analysis Translator ver. 3.10, Reference Manual - IETiME PW 1991.

[13] Field Analysis Translator ver. 3.10, User's Guide - IETiME PW 1991.

Elżbieta Ratajewicz-Mikołajczak and Zbigniew Złonkiewicz
Lublin Technical University

ENVIRONMENT FRIENDLY PRESENT-DAY ELECTROTECHNOLOGICAL PROCESSES

Introduction

Electrotechnological processes are generally friendly for environment. Some of these are used directly to protect the environment, for example: electrostastic dust removal or magnetic separation. Other modern electrotechnologies in comparison with conventional production technologies are characterized by small energy consumption. They often generate less or even no waste products, reduce dust emission to the atmosphere and eliminate agents harmful for the human organism and environment. Some of these electrotechnologies are presented.

Plasma treatment

In plasma treatment the ionised gas flux is used for technological purposes. In the contact with treated material the plasma flux reaches very high temperature (4000 - 17000 K). The temperature distribution in the plasma flux is seen on the fig. 1.

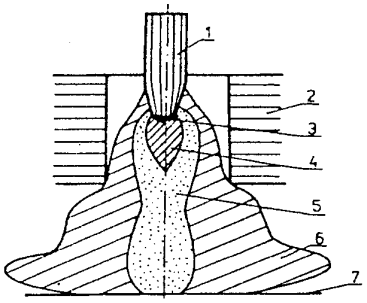

Fig.1. The temperature distribution in the plasma flux: 1 - tungsten cathode, 2 - nozzle (copper anode with water cooling), 3 - zone of temperature higher then 20000K, 4 - zone of temperature in the range of 17000 - 20000 K, 5 - zone of temperature in the range of 15000 - 17000 K, 6 - zone of temperature in the range of 10000 - 15000 K, 7 - treated material.

There are many methodes of plasma generation such as the chemical or nuclear explosions, shock waves and electric discharge. The electric discharge is used mainly in industrial plasmatrons. Higher power of these plasmatrons is 10^7 W.

The high power density enables using the plasma treatment for metal cutting, coating, metal melting or receiving of monocrystals. These processes are environment friendly because often they do not give any waste products

Plasma melting furnances used for high-melting materials are characterized by significant reduction of dust in comparison with conventional furnances.

The example of plasma application in the metallurgical industry is the plasma arc furnance presented in Fig. 2.

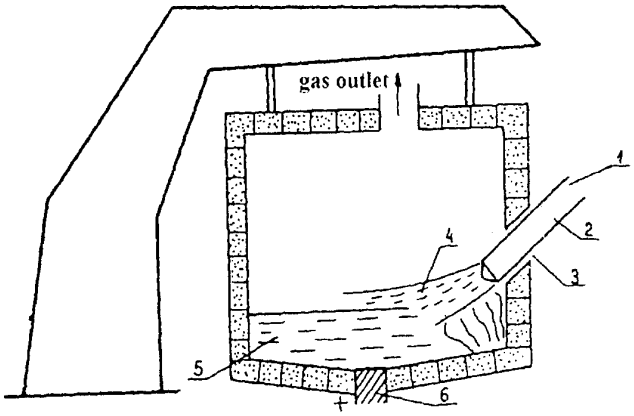

Fig.2.. The plasma arc furnance: 1 - plasmatron, 2 - cathode, 3 - nozzle, 4 - area of plasma, 5 - melt, 6 - anode

Typical parameters of the plasma furnences:

Power	160 - 2000 kW
Voltage	40 - 200 V
Mass of the melt	max 5000 kg

Laser Treatment

As the result of a high density flux of photons the treated material is melted and evaporated. The temperature in this place is 5200 - 8700 K. The source of the coherent light beam in this kind of machining is a gas laser, a liquid laser, a ruby crystal laser or a semiconductor laser. It is possible that the light beam power of the synthetic ruby laser is 100 kW in 10 μs. The laser treatment is very precise because the light beam is very focused and its heat flux is very dense. The laser treatment is one of the processes which generate less or even no waste products. It is possible to provide this machining covered under glassshields and eleminate all pollutants and agents harmful for the human organism.

The application examples of pulsed lasers are seen in the table below.

Tab. Typical parameters and applications of the pulsed lasers.

Type of the pulsed laser	Wavelenght 10(μm)	Impuls energy (J)	Frequency of impulses (Hz)	Efficiency (%)	Power (W)	Application
CO_2	10.6	0.1 - 30000	2500 (max)	5 - 15	3000	cutting, drilling, welding
TEA - CO_2	10.6	0.03 - 75	0.1 - 300	1 - 10	200	engraving, hardening
Nd - YAG	1.64	0.01 - 100	0.05 - 300	0.1 - 2	400	cuting, drilling, marking
Nd glass	1.06	0.15 - 100	0.1 - 1	1.5	40	welding, drilling

Technical Application of Electrokinetic Phenomena

The elektrokinetic phenomena which are especially important found many applications for environment protection in electrodeposition of paint which is used on a large scale in the present day industry. The dilution of paints with water eliminates the harmfulness of organic solvents for the environment.

The idea of the electropforetic painting is the following: the part, which should be coated, is dipped in the diluted paint and connected to the power source as one electrode. The second electrode is a metallic tank. After turning on of voltage the resin and the pigment migrate ti the dipped part and make the coat.

Most often is used direct voltage 100 - 250V and current density 20 - 100A/m^2. The coating time is 60 -180s and the thickness of coat - 25 - 35mm.The scheme of the tank is seen of the fig.3

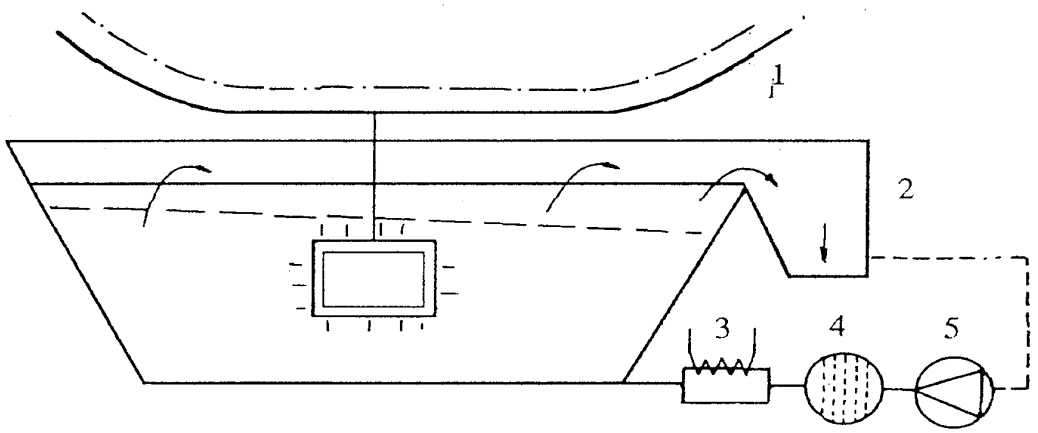

Fig. 3. Electrophoretic coating: 1 - overhead conveyor and contact rail, 2 - overflow, 3 - heat exchanger, 4 - filter, 5 - pump

Summary

There are many modern electrotechnological processes characterized by small energy consumption, no waste products and reduction of dust emmision to the atmosphere. A few of these are commented.

Electrotechnological processes are used to product, store and convert electrical energy. The reports from many countries of the investigation on the field of electrochemical induced cold fusion are interesting. The effect cannot yet be reliably reproduced at request. It can not be used in practice now and soon, but one could hope that after some progress in investigations this effect may introduce the revolution in the world energy production.

References

1. H. Conrad, R. Krampitz : Elektrotechnologie. VEB Verlag Technik, Berlin 1983.

2. Praca zbiorowa : Chemia plazmy niskotemperaturowej . Warszawa, WNT 1983.

3. Katalog Societe Nouvelle de Metallisation Industries Boite Postale N^{O} 205 - 84500 BOLLENE - France : Industrial Use of Plasma Transferred Arc Hardfacing

4. T. Burakowski, J. Strauss : Rozwój techniki laserowej dla potrzeb technologicznych. Metaloznastwo. Obróbka cieplna. Inżynieria powierzchni Nr88, lipiec- sierpień 1987.

5. Trzęsowski Z. : Lasery technologiczne CO_2 dużej mocy. Część I - Przegląd rozwiązań Metaloznastwo. Obróbka cieplna. Inżynieria powierzchni Nr88, lipiec- sierpień 1987.

6. Trzęsowski Z. : Lasery technologiczne CO_2 dużej mocy. Część II - Lasery z dyfuzyjną stabilizacją wyładowania.Metaloznastwo. Obróbka cieplna. Inżynieria powierzchni Nr88, lipiec- sierpień 1987.

7. Szczepański Z., Banasik M.: Wykorzystanie laserów do cięcia i spawania materiałów. Metaloznastwo. Obróbka cieplna. Inżynieria powierzchni Nr88, lipiec- sierpień 1987.

8. Koichi. B., Shimoda H. - Wstęp do fizyki laserów. PWN Warszawa 1993.

9. W. Dembiński i inni : Search for the cold nuclear fusion .(Verification of Fleischman and Pons experiments), Institute of Nuclear Chemistry and Technology, Warszawa 1990.

10. Johnson M.: Futher Evidence for Cold Fussion - a Report on the Third International Conference, Platinum Metals Review, Nr 1, Jan.1993.

Krzysztof Kawka and Paweł Surdacki
Lublin Technical University, Dept. of Fundamental Electrical Engineering, Poland

MAGNETIC FORCES AND MECHANICAL STRESSES IN SUPERCONDUCTING WINDINGS OF CRYOMAGNET

1. Introduction

It is required to compute thermal, electrical, magnetic and mechanical parameters during the designing of superconducting magnet systems.

Mechanical parameters such as forces, stresses, deformations and strength are important during a consideration of a superconductivity disturbance condition. The disturbance can be caused by excessive mechanical stresses causing small relative coil shifts and micro-crackings of superconducting wire and an insulation. This results in heat impulses delivered to the winding which can result in a superconductor's degradation and local transitions into a resistive state [3,7].

Cryomagnet stresses are caused by mechanical forces generated during a winding coil process, thermo-mechanical forces caused by cooling to cryogenic temperatures and by electrodynamic forces [5,6].

In superconducting magnets characterized by a magnetic field high concentration and current density a few orders higher than in common magnets, the electrodynamic forces can reach very high values [1]. Such large forces can cause superconductivity decay and windings and structural elements can get damaged.

The paper considers some first approach to computations of magnetic forces and the resulting mechanical stresses in the cryomagnet winding in steady state. Common designing assumes averaged or even simplified distributions of magnetic field in the winding [4,7]. The method based on computations of a real magnetic field distribution in the winding is proposed in the paper to generalize the considerations on windings of finite width and length.

2. Stresses and force balance conditions

Let us consider an elementary cell of the homogeneous cylindrical winding in a cylindrical coordinate system. The parameters of the winding are: R_1 - internal radius, R_2 - external radius, L - length. All stresses occuring in the elementary cylinder cutting are shown in the Fig. 1.

Force balance conditions for a cylinder cutting have the following forms [2]:

A) along the radius

$$\left(\sigma_r + \frac{\partial \sigma_r}{\partial r} dr\right) dx (r + dr) d\theta - \sigma_r dx\, r\, d\theta + \left(\tau_{xr} + \frac{\partial \tau_{xr}}{\partial x} dx\right) \frac{1}{2} dr\left[r d\theta + d\theta (r + dr)\right] -$$

$$- \frac{1}{2} \tau_{xr} dr\left[r d\theta + d\theta (r + dr)\right] - \sigma_\theta\, dr\, dx\, d\theta + rR\, dx\, dr\, d\theta = 0, \qquad (1)$$

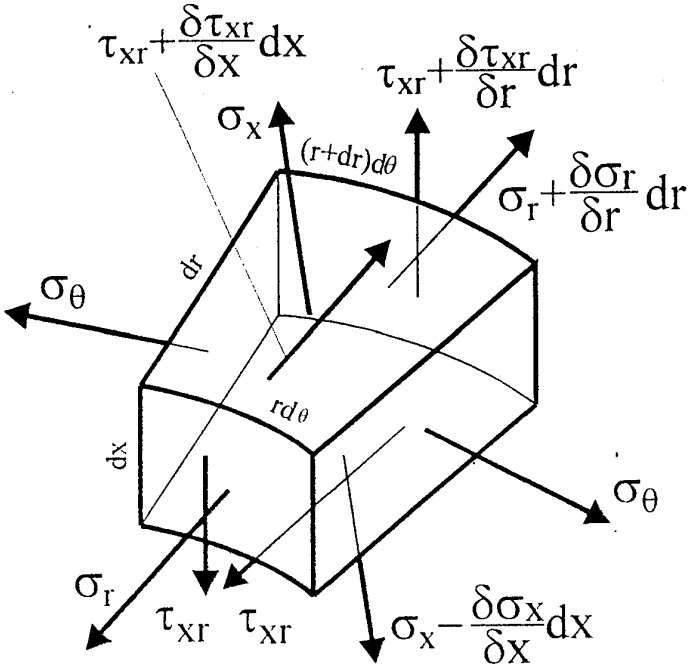

Fig. 1. Stresses in the elementary cell of the winding; where: r - radial coordinate of the winding, z - axial coordinate, θ - angular coordinate, σ_r - normal radial stress, σ_x - normal axial stress, σ_θ - normal circumferential stress, τ_{xr} - shearing stress, R - radial component of a force acting on elementary cell of volume r dr dz dθ, S - axial component of this force.

B) along the axis

$$\left(\tau_{xr}+\frac{\partial\tau_{xr}}{\partial r}dr\right)\left[(r+dr)d\theta dx\right]-\tau_{xr}rd\theta dx+\frac{1}{2}(2r+dr)d\theta dr\left(\sigma_x-\sigma_x+\frac{\partial\sigma_x}{\partial x}dx\right)+Srdx\,dr\,d\theta=0. \quad (2)$$

From the equation (1) and (2) we obtain the following equations of the balance for an elementary cell of the winding:

$$r\left(\frac{\partial\sigma_r}{\partial r}+\frac{\partial\tau_{xr}}{\partial x}\right)+\sigma_r-\sigma_\theta+rR=0 \quad (3)$$

$$r\left(\frac{\partial\sigma_x}{\partial x}+\frac{\partial\tau_{xr}}{\partial r}\right)+\tau_{xr}+rS=0 \quad (4)$$

3. Analytical formulas for stresses

Lets us accept the following assumptions for the cylindrical winding::

- Due to symmetry, tangential stress τ_{xr}, derivative $\frac{\partial\tau_{xr}}{\partial r}$ and force S have zero values in the midplane of the winding,
- normal axial stresses are neglected and the problem is 2-dimensional, where only radial forces act.

A differential equation of stress function is taken simalarly as in [2].

Simplifying (3) and (4) we obtain:

$$r\frac{\partial\sigma_r}{\partial r}+\sigma_r-\sigma_\theta+rR=0 \tag{5}$$

Formula (5) can be written as:

$$r\frac{\partial(r\sigma_r)}{\partial r}-\sigma_\theta+rR=0 \tag{6}$$

From the Hooke law for a planar system we have:

$$\varepsilon_r=\frac{1}{E}(\sigma_r+\nu\sigma_\theta) \tag{7}$$

$$\varepsilon_\theta=\frac{1}{E}(\sigma_\theta+\nu\sigma_r) \tag{8}$$

where: ε_r, ε_θ - components of strain tensor, ν - a material constant.

Strain tensor in polar coordinates has the form:

$$\varepsilon_r=\frac{\partial u_r}{\partial r} \tag{9}$$

$$\varepsilon_\varphi=\frac{1}{r}\frac{\partial u_\varphi}{\partial\varphi}+\frac{u_r}{r} \tag{10}$$

where: u_r, u_φ: radial and circumferential displacements, respectively,

Due to a symmetry of magnetic field in a relation to an axis, we accept $u_\varphi = 0$. So formula (10) is simplified to the following:

$$\varepsilon_{\varphi\varphi}=\frac{u_r}{r} \tag{11}$$

We put the formulas (7) and (9) into equation (12) of matter's continuity:

$$\varepsilon_\theta-\varepsilon_r+r\frac{d\varepsilon_\theta}{dr} \tag{12}$$

In order to obtain relevant stresses from the equations (6), (7), (8) and (12), We introduce an additional function $f=\sigma_r r$, from which

$$\sigma_r=\frac{f}{r} \tag{13}$$

Putting function f into (6) we have:

$$\sigma_\theta=\frac{df}{dr}+rR \tag{14}$$

and putting (13) and (14) into (7), (8) we obtain:

$$\varepsilon_r=\frac{1}{E}\left(\frac{f}{r}+\nu\left(\frac{df}{dr}+rR\right)\right) \tag{15}$$

$$\varepsilon_\theta=\frac{1}{E}\left(\frac{df}{dr}+rR+\nu\frac{f}{r}\right) \tag{16}$$

Taking into account the medium continuity condition, we obtain:

$$\frac{d^2f}{dr^2}+\frac{1}{r}\frac{df}{dr}-\frac{f}{r^2}=\left[(2+\nu)R+r\frac{dR}{dr}\right] \tag{17}$$

$$B_x(r) = -116.011r + 13.937 \tag{20}$$

Force acting on elementary cell of the winding:

$$R(r) = B_x(r)J \tag{21}$$

Taking (20) and (21) into the formulas (18) and (19) we obtain distributions of σ_θ and σ_r represented by fig. 3 and fig. 4.

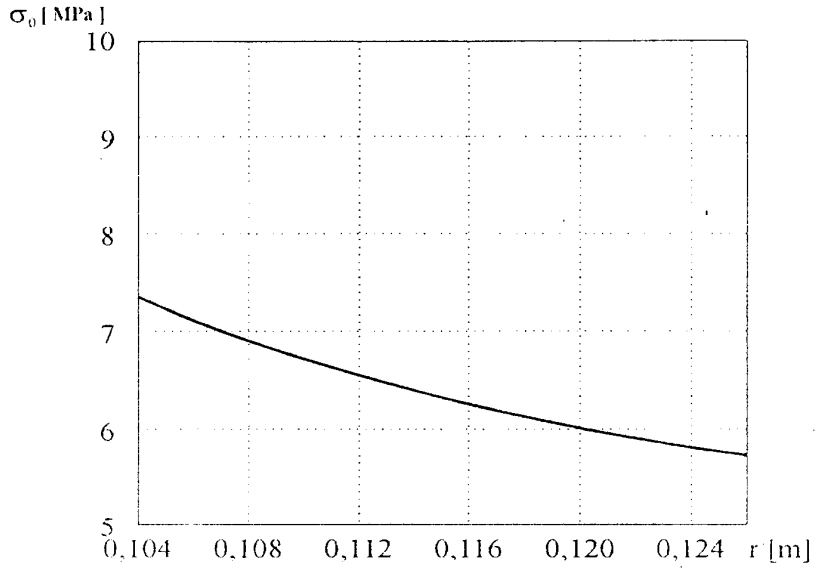

Fig. 3. Circumferential stress σ_θ as a radius function.

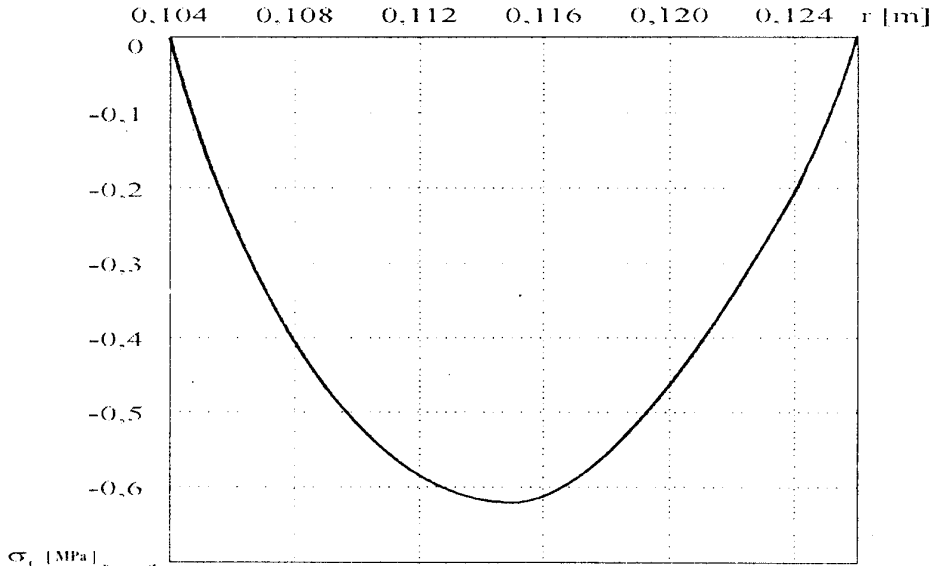

Fig. 4. Radial stress σ_r as a radius function.

The solution for the boundary conditions $\sigma_r(r_1) = 0$ and $\sigma_r(r_2) = 0$:

$$\sigma_r = \frac{1}{2}\left\{ \frac{1}{r_2^2 - r_1^2}\left(1 - \frac{r_1^2}{r^2}\right)\left[(1+\nu)r_2^2\int_{r_1}^{r_2} Rdr + (1-\nu)\int_{r_1}^{r_2} r^2 Rdr\right] - (1+\nu)\int_{r_1}^{r} Rdr - \frac{(1-\nu)}{r^2}\int_{r_1}^{r} r^2 Rdr \right\} \quad (18)$$

$$\sigma_r = \frac{1}{2}\left\{ \frac{1}{r_2^2 - r_1^2}\left(1 + \frac{r_1^2}{r^2}\right)\left[(1+\nu)r_2^2\int_{r_1}^{r_2} Rdr + (1-\nu)\int_{r_1}^{r_2} r^2 Rdr\right] - (1+\nu)\int_{r_1}^{r} Rdr + \frac{(1-\nu)}{r^2}\int_{r_1}^{r} r^2 Rdr \right\} \quad (19)$$

4. Evaluation of magnetic field and stresses

In order to evaluate mechanical stresses caused by radial component of magnetic force R occuring in (18) and (19) we have to compute distribution of magnetic flux density axial component $B_X(r,x)$. Computations has been performed for the following winding's parameters: internal radius $R_1 = 0.104$ m, external radius $R_2 = 0.126$ m, winding thickness $d = 0.022$ m, length $L = 0.111$ m, at normalized current density of $J = 10^8$ A/m^2. The FEM2D package has been implemented to solve 2-dimentional axisymmetrical problem by means of Finite Element Method. The computational results (Fig. 2) make possible to approximate $B_X(r)$ distribution for the winding midplane (x=0):

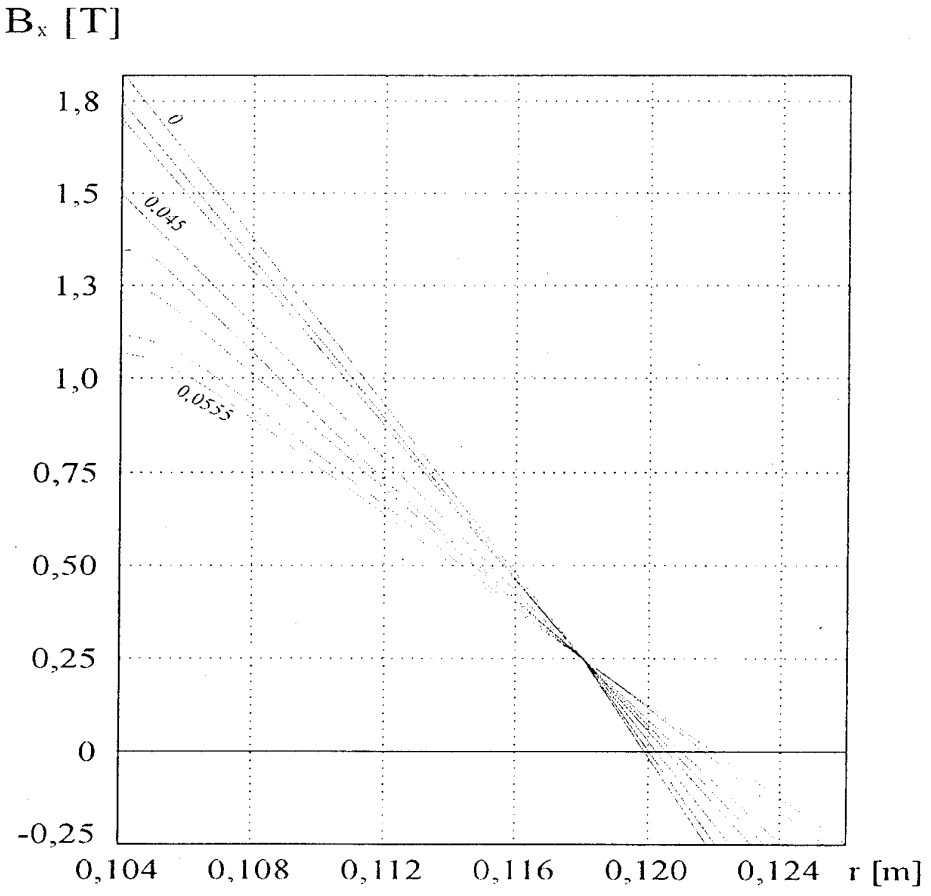

Fig. 2. Distribution of magnetic flux density axial component along a radius at various distances x from winding symmetry axis computed by means of FEM2D package.

5. Discussion of the results

In performed example, stresses in the winding of reduced radius

$$\eta = \frac{R_2 - R_1}{R_1} = 0.2115 \tag{22}$$

were calculated. For other values of η the calculation procedure is similar, but the results can be quite different [3].

In our example, normal radial stress function $\sigma_r(r)$ has negative values in a whole segment of thickness from R_1 to R_2, i.e. the winding is compressed. The lowest value $\sigma_{rmin} = 0.6812 \cdot 10^6$ Pa of radial stress is at $r = 0.115$ m.

The highest circumferential stress occurs at $r = R_1$ and has its value $\sigma_{\theta max} = 7.35 \cdot 10^6$ Pa.

The presented procedure involving the equations (18) and (19) of stresses σ_θ and σ_r are only approximate, however may be succesfully used in the first stage of cylindrical winding stress evaluation and designing processes.

References:

[1] Middleton A.J., Trowbridge, Mechanical Stress in Large High Field Magnet Coils, Proc. Intern Symp. on Magnet Technology, Rutherford Laboratory, Didcot, England, p 140., 1967

[2] Huber M.T., **Theory of Elasticity,** Part I, PWN Warszawa, 1954 (in Polish).

[3] Kazowskij E.Ja., Karcew W.P., Szachtarin W.N.; **Svierchprowodjaszczije magnitnyje sistemy**; Izdatielstwo "Nauka", Leningrad; 1967.

[4] Montgomery D.B.; **Solenoid Magnet Design**; John Wiley & Sons, New York; 1969.

[5] Okada S., Iwahashi Y., Mori H.; A Practical Structural Stress Evaluation System for Superconducting Coils with Inner Ring Support; **Int. Journ. of Applied Electro magnetics in Materials**, 1, pp. 99-108; 1990.

[6] Thome and J.M. Tarah; MHD and Fusion Magnets, Field and Force Concepts, Wiley, New York, pp 180-201; 1980.

[7] Wilson M.N.; **Superconducting Magnets**; Clarendon Press, Oxford; 1983.

Paweł Surdacki

Lublin Technical University

APPROACH TO THERMAL ANALYSIS OF SUPERCONDUCTING DEVICE CURRENT LEADS

1. Introduction

Current leads of some large superconducting magnets are decisive for their quality and performance. They also influence cryostat dimensions and indispensable efficiency of cryocooling system. In particular, they influence a cryomagnet work in transients. Lead's optimal dimensions are determined by electromagnetic and thermal phenomena not only in the very leads but also in windings and structural parts of cryomagnets [5,7].

Connection between a cryomagnet winding and a supplying system is worked out by means of cryoleads. While it is submerged in liquid helium of working temperature about 4 K, its joint with supplying system is placed on the cryostat cover of environment temperature about 290 K [1].

For such a considerable temperature difference, the current lead must be long sufficiently to minimize temperature gradient. This makes necessary to lenghten the cryostat that increase its price, heat amount conducting to liquid helium and helium evaporation [6].

Lead resistivity at such large temperature differences changes along its length and lead cross-section can be variable to maintain acceptable power loss density. In large current cryomagnets, the leads can reach considerable sizes and are a main way to heat transfer into cryostat inside [2].

In this paper, a first approach to a thermal analysis is presented for two groups of superconducting device current leads: thermally insulated and cooled by cryogenic liquids and vapours. Considerations have been worked out for steady states.

2. Insulated current leads

Considerations on heat flow from higher temperature T_C to lower temperature T_Z area through current leads are based on two equations [4]:

- Joule's equation, heat quantity generating in a time unit in a lead element flowing a current:

$$d\dot{Q} = I^2 \frac{dx}{\gamma\ s} \tag{1}$$

- Fourier's equation, heat flow for steady conducting:

$$\dot{Q} = -\lambda\, s \frac{dt}{dx} \tag{2}$$

where: Q - heat flow, [W], I - electrical current [A], γ - conductivity [$\Omega^{-1}\cdot m^{-1}$], s - lead cross-section area [m^2], x - variable lead length [m], T - temperature [K], λ - thermal conductivity [$W\cdot m^{-1}\cdot deg^{-1}$].

In a case of a small temperature gradient ($\Delta T = T_C - T_Z$), thermal conductivity and electrical conductivity have been accepted as a constant: λ = const., ρ = const.

From these equations, after some transformations, we get temperature

$$T_x = T_c - \frac{1}{\lambda\, s}\left(\frac{I^2 x^2}{2\,\gamma\, s} + \dot{Q}_c\, x\right) \tag{3}$$

and then heat flow intensity at distance x from warm end

$$\dot{Q}_c = \frac{\Delta T \lambda s}{L} + \frac{I^2}{\gamma s}\left(x - \frac{L}{2}\right) \tag{4}$$

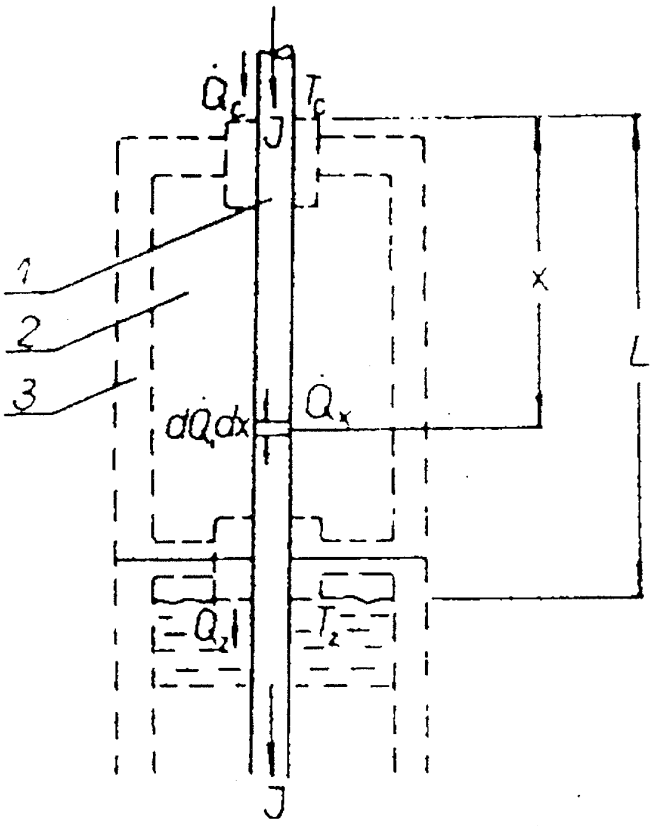

Fig. 1. Heat exchange in cryogenic current lead insulated thermically;
1 - current lead, 2 - vacuum insulation of heat, 3 - cryostat.

Depending on electric current, we have three cases for quantity Q_C, heat flow and way of a temperature calculation:

1) the small relative value of current, $\dot{Q}_C > 0$, heat flows into the lead from its warm end,

$$\text{when } \frac{\Delta T \lambda s}{L} > \frac{I^2 L}{2\gamma s} \tag{5}$$

$$T_x = T_c - \frac{I^2 x^2}{2\gamma\lambda s^2} - \frac{x}{\lambda s}\left(\frac{\Delta T \lambda s}{L} - \frac{I^2 L}{2\gamma s}\right) \tag{6}$$

2) the optimum value of current, $\dot{Q}_c = 0$, no heat flow in warm end of the lead,

$$\text{when } \frac{\Delta T \lambda s}{L} = \frac{I^2 L}{2\gamma s} \tag{7}$$

$$T_x = T_c - \frac{I^2 x^2}{2\gamma\lambda s^2} \tag{8}$$

3) the large relative value of current, $\dot{Q}_c < 0$, heat flows out of the warm end of the lead.

$$\text{when } \frac{\Delta T \lambda s}{L} < \frac{I^2 L}{2\gamma s} \tag{9}$$

$$T_x = T_c + I^2 \cdot \frac{Lx - x^2}{2\gamma\lambda s^2} - \frac{\Delta T}{L} x \tag{10}$$

Heat flow intensity for the all cases is described by a formula

$$\dot{Q}_z = \frac{\Delta T \lambda s}{L} + \frac{I^2 L}{2\gamma s} \tag{11}$$

and hence its dependence on resistance has a form

$$\dot{Q}_z = \frac{\Delta T \lambda}{R\gamma} + \frac{I^2 R}{2} \tag{12}$$

Minimum of this function is, when

$$-\frac{\Delta T \lambda}{R^2 \gamma} + \frac{I^2}{2} = 0 \tag{13}$$

so the value of resistance is

$$R = \frac{1}{I}\sqrt{\frac{2\Delta T}{\gamma}} \tag{14}$$

and minimum of heat transfer by the lead's warm end is

$$\dot{Q}_{z\min} = I\sqrt{\frac{2\Delta T \lambda}{\gamma}}. \tag{15}$$

Therefore, there exists the minimum of heat transfer intensity of the lead's cold end in the case of a specific value of lead resistance and for the given cross-section s lead's length is

$$L = R\gamma s = \frac{s}{I}\sqrt{2\Delta T \lambda \gamma}. \tag{16}$$

In the case of the large temperature gradient it is necessary to take into account temperature dependence of thermal conductivity and electric conductivity

$$\lambda = \text{var} = f_1(T) \qquad \rho = \text{var} = f_2(T). \tag{17}$$

In this case, heat transfer intensity is described by the formula

$$\dot{Q}_{z\,min} = I\sqrt{2\int_{T_z}^{T_c}\frac{\lambda}{\gamma}dT}. \tag{18}$$

Lead's resisivity can be calculated from the formula

$$R = \sqrt{2\int_{T_z}^{T_c}\frac{\lambda}{\gamma}dT} \tag{19}$$

and its length for the given coss-section from the formula

$$L = \frac{s}{I}\sqrt{2\int_{T_z}^{T_c}\lambda\gamma\,dT}. \tag{20}$$

3. Gas-cooled current leads

In the gas-cooled current leads, vapours of a cryogenic liquid are used to cool a lead's side surface (Figure 2).

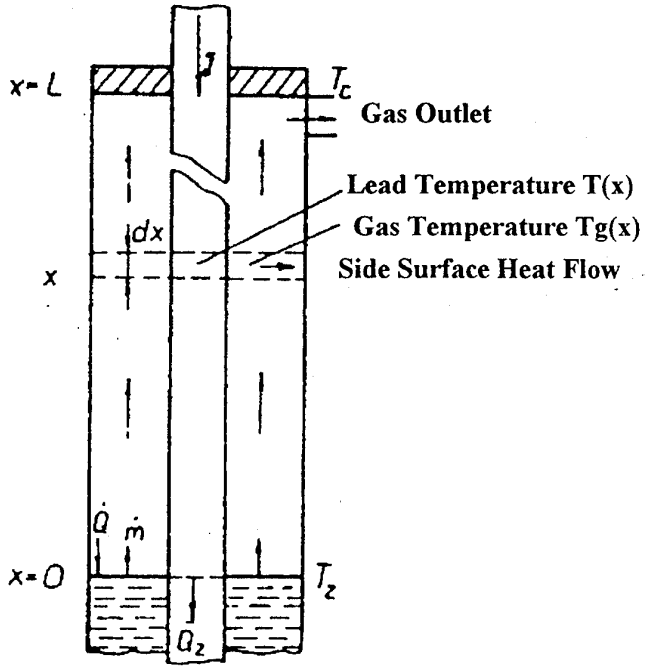

Fig. 2. Current lead cooled by vapours of a cryogenic liquid.

A heat balance for this case is by the following system of differential equations:

$$\frac{d}{dx}\left[\lambda(T)\,s(x)\frac{dT}{dx}\right] + \frac{I^2\,\rho(T)}{s(x)} = h(T)\,p(x)(T - T_g) \tag{21}$$

$$h(T)\,p(x)(T - T_g) = \dot{m}c_p(T)\frac{dT}{dx} \tag{22}$$

where: h(T) - coefficient of a heat transfer between the lead and the gas, p(x) - perimeter of the current lead, s(x) - cross-section of the current lead, T_g - gas temperature, $\rho(T)$ - resistivity

of lead's material, Q_Z - heat flow along the current lead, Q_K - heat flow along cryostat walls, r - evaporation heat of a coolant, m - intensity of the gas flow along the lead, given by

$$\dot{m} = \frac{\dot{Q}_z + \dot{Q}_k}{r} \tag{23}$$

A quantity of heat flowing to the liquid along the current flow is described by the formula

$$Q_z(T_z) = -\lambda(T_z)\, s(z) \left.\frac{dT}{dx}\right|_{x=0} . \tag{24}$$

The following boundary conditions should be taken into consideration to solve the system of (21) and (22):

$$\begin{aligned} T(0) &= T_g(0) = T_Z \\ T(L) &= T_C . \end{aligned} \tag{25}$$

4. Final remark

In the case of the insulated current leads, it is easy to obtain some analytical expressions for a temperature distribution and optimal parameters.

However, in order to find parameters necessary to design the gas-cooled cryogenic current leads, the efficient computer code should be worked out for differential equation system solution. The computation should take into account some temperature-dependent material and cryocooler parameters.

In recent superconducting devices, there are also some superconducting current leads applied instead of the classical copper leads [3]. They should be also analyzed in near future in order to obtain their optimal parameters.

References:

[1] Bartenev V.D., Shishov Yu.A.; Force-cooled current leads for the force-cooled superconducting magnets of the Nuclotron; **Cryogenics**, Vol. 31, No.11, November, pp. 985 - 987; 1991;

[2] Gerhold J.; Design criteria for high voltage leads for superconducting power systems; **Cryogenics**, Vol. 24, February, pp. 73-82; 1984.

[3] Hull J.R., Unal A., Chyu M.C.; Analysis of self-cooled binary current leads containing high temperature superconductors; **Cryogenics**, Vol. 32, No. 9, pp. 822-828; 1992.

[4] Janiczek S.; Cryoelectrotechnics foundations (in Polish); **Politechnika Częstochowska Publishers**, Częstochowa; 1993.

[5] Koefler H., Ramsauer F.; Influence of Copper Quality on Overload Performance of Current Leads; **Cryogenics**, Vol. 32, ICEC Supplement, pp. 410-413; 1992.

[6] Samorodov I.I., Filatov V.V.; Optimization of an Independently Cooled Cryogenic Current Lead; **Cryogenics**, Vol. 32, ICEC Supplement, pp. 414-4418; 1992.

[7] Wilson M.N.; Stabilization, protection and current density: some general observations and speculations; **Cryogenics**, Vol. 31, July, pp. 499-503; 1991.

ISBN 83-86333-01-4